

# A NOVEL IMPLEMENTATION OF CONCURRENT SENSING IN SWEAT OR BLOOD

Keming Chen  
CID: 01897064

*Supervised by:*  
*Prof. Pantelis Georgiou*

*Co-supervised by:*  
*Daryl Ma*

A Thesis submitted in fulfilment of requirements for the degree of  
Master of Science  
Analogue and Digital Integrated Circuit Design  
of Imperial College London

Department of Electrical and Electronic Engineering  
Imperial College London  
September 2, 2021

## Abstract

Electrochemical biosensors are of great importance to modern healthcare applications containing large amount of commercial value due to their advantages in fast time response, low cost and potential for miniaturization. This thesis first introduces detailed background of the electrochemical biosensors and relevant common techniques of electrical signal readout and then focus on designing a novel implementation of concurrent sensing in bio-fluid.

The projects involves the introduction of the initial design of the dual amperometric and potentiometric sensing front end circuits with single channel output through a digital mixing block. The qualitative analysis mainly focus on characterization of the potentiometry and amperometry in linearity, input dynamic range, power consumption and sensitivity, etc.

A improved amperometric and potentiometric circuitry are simulated in TSMC180BCD technology and presented to have improvement on potentiometric dynamic input range from 0.4 - 1V to 0.2 to 1.2V and amperometric dynamic input range from 80p-1uA to 158p-6uA. Maximum power consumption drops from 16.71uW to 7.63uW under the same testing condition when input is 1V and the input current is 0.5uA.

## Acknowledgements

I would like to give gratitude to Dr. Pantelis Georgiou for providing this opportunity to do this project. Apart from that lecture contents in Analog Signal Processing he taught in the class is very useful which helps me understand the analog circuits deeply and make me read literature easier.

I would also like to give a great appreciation to my co-supervisor Daryl Ma who was the helping me a lot and giving out valuable advice whenever I needed. Although I did not make some progress and have no direction at some points due to complex reasons, Daryl are kind to provide opportunities on chip testing which improves my hands-on ability as well as understanding the Project itself. Thanks for helping me out whether mentally and physically going through those tough time.

Furthermore I would like to give special thanks to my coursemates who offer me many advice on both academic and career aspects.

Last but not the least, I would thank to my parents for supporting me financially and spiritually.

# Contents

<b>Abstract</b>	<b>i</b>
<b>Acknowledgements</b>	<b>ii</b>
<b>Contents</b>	<b>iii</b>
<b>List of Tables</b>	<b>vi</b>
<b>List of Figures</b>	<b>vii</b>
<b>Abbreviations</b>	<b>x</b>
<b>1 Introduction</b>	<b>1</b>
1.1 Motivation . . . . .	1
1.2 objectives . . . . .	2
1.3 Thesis Outline . . . . .	3
<b>2 Background Theory</b>	<b>4</b>
2.1 Biosensor . . . . .	4
2.2 Electrochemical Biosensor techniques . . . . .	5

2.2.1	Potentiometric biosensor . . . . .	6
2.2.2	Amperometric biosensor . . . . .	7
2.2.3	Impedimetric biosensor . . . . .	8
2.2.4	Ion-sensitive Field Effect Transistor Biosensor . . . . .	9
2.3	Electrode transducer . . . . .	10
2.4	CMOS instrumentation for amperometric and potentiometric biosensors . . . .	12
2.4.1	Potentiostat . . . . .	14
2.4.2	Readout circuitry . . . . .	16
<b>3</b>	<b>Initial design of potentiometry and Amperometry</b>	<b>27</b>
3.1	Overall structure . . . . .	27
3.2	potentiostat with shared reference electrodes . . . . .	29
3.3	Potentiometry . . . . .	31
3.3.1	Voltage to current converter . . . . .	32
3.3.2	Current starved ring oscillator . . . . .	36
3.4	Amperometry . . . . .	40
3.5	Mixing signal . . . . .	43
<b>4</b>	<b>Improved potentiometric and amperometric readout circuits system</b>	<b>45</b>
4.1	Adapted voltage to current converter . . . . .	45
4.1.1	Structures . . . . .	45
4.1.2	Principles . . . . .	46

---

4.1.3	Simulation results . . . . .	49
4.2	Improved current controlled oscillator in amperometry . . . . .	51
4.2.1	Simulation results . . . . .	57
4.3	improved current controlled oscillator for potentiometry . . . . .	60
4.3.1	Structures . . . . .	60
4.3.2	Principles . . . . .	61
4.3.3	simulation results . . . . .	65
4.3.4	Overall simulation results . . . . .	67
<b>5</b>	<b>Conclusion</b>	<b>69</b>
5.1	Conclusion . . . . .	69
5.2	Future Work . . . . .	70
	<b>Bibliography</b>	<b>71</b>

# List of Tables

4.1	Sizes of transistors in the voltage-to-current converter circuits . . . . .	50
4.2	Sizes of transistors in the current controlled oscillator . . . . .	57
4.3	Sizes of transistors in the current to voltage converter . . . . .	65
4.4	Sizes of transistors in the current to voltage converter . . . . .	68

# List of Figures

2.1	Electrochemical biosensor structure . . . . .	6
2.2	Potentiometric measurement [1] . . . . .	7
2.3	Amperometric measurement [1] . . . . .	8
2.4	The charge profile of the electrode-electrolyte interface [2] . . . . .	9
2.5	Structure of ISFET. It consists of source, drain, gate insulator, and reference electrode. [3] . . . . .	10
2.6	Simple schematic of two electrode configuration. [4] . . . . .	11
2.7	Simple schematic of three electrode configuration. [4] . . . . .	12
2.8	Instrumentation circuit in potentiometry. . . . .	13
2.9	The structure of the instrumentation for electrochemical biosensors. . . . .	14
2.10	Three-electrode potentiostat with the grounded-WE structure. . . . .	15
2.11	Three-electrode potentiostat with the grounded-CE structure. . . . .	16
2.12	The schematic of DC voltage readout circuit[5] . . . . .	17
2.13	Resistive feedback current readout circuit . . . . .	19
2.14	Capacitive feedback current readout circuit . . . . .	19
2.15	Structure of correlation double sampling circuit . . . . .	21

2.16	Structure of current conveyor circuit . . . . .	21
2.17	Structure of current conveyor circuit with current source/sink . . . . .	22
2.18	Structure of a first-order incremental current mode ADC circuit for amperometric sensing . . . . .	23
2.19	First-order incremental current mode $\Sigma \Delta$ ADC circuit in application . . . . .	24
2.20	Output waveform of flip flop and integrator without input current[6] . . . . .	26
2.21	Output waveform of flip flop and integrator with input current [6] . . . . .	26
3.1	The overall structure of proposed sensor . . . . .	27
3.2	The structure of potentiostat with shared reference . . . . .	31
3.3	The structure of potentiometric circuitry . . . . .	32
3.4	The equivalent digital model of inverter[7] . . . . .	36
3.5	Schematic of potentiometric circuit . . . . .	38
3.6	Digital model of inverter in current startedved ring oscillator . . . . .	39
3.7	Waveform of amperometric output . . . . .	41
3.8	Waveform of mixed signal . . . . .	43
4.1	Structure of voltage-to-current converter . . . . .	45
4.2	Schematic of adapted voltage-to-current converter . . . . .	46
4.3	Converted current vs input voltage . . . . .	50
4.4	Structure of improved current controlled oscillator . . . . .	51
4.5	Digital model of inverter in improved current controlled oscillator . . . . .	52
4.6	Schematic of improved current controlled oscillator . . . . .	54

---

4.7	Output waveform of improved current controlled oscillator . . . . .	55
4.8	Systematic simulation results for current-to-frequency . . . . .	58
4.9	Power consumption in current-to-frequency converter . . . . .	58
4.10	Ideal curve versus simulated curve . . . . .	59
4.11	Current controlled oscillator with reference voltage . . . . .	60
4.12	Schematic of PMOS comparator . . . . .	61
4.13	Waveform of renewed current controlled oscillator . . . . .	63
4.14	Systematic simulation on potentiometric circuit . . . . .	66
4.15	Power consumption of potentiometric circuit . . . . .	67

# Abbreviations

ISFET	Ionization Sensitive Field Effect Transistor
MOSFET	Metal Oxide Semiconductor Field Effect Transistor
CMOS	Complementary MOSFET
RE	reference electrode
WE	working electrode
CE	counter electrode
ISE	Ion-sensitive electrode
DNA	Deoxyribose Nucleic Acid
pH	Power of Hydrogen
LIF	Leaky Integrate and Fire
CDS	Correlated Double Sampling
ADC	Digital-to-Analog Converter
DAC	Digital-to-Analog Converter
PCB	Printed Circuit Board

# Chapter 1

## Introduction

### 1.1 Motivation

RECENT research has revealed that for some common chronic diseases including cancer, diabetes, cardiovascular diseases, which contributes to many death and disability, apart from leading a healthy personal lifestyle, prevention to that potential illness would be diagnosis at an early stage, which heavily relies on the consistent body fluid checking at the hospital, expensive, inconvenient and time consuming since body fluid analysis depends on the bulky medical diagnostic instrument in hospital while increasing the burden of the healthcare system[8]. Therefore, with the evolution of Internet of Things(IoT), the win-win method comes up by developing remote monitoring on the body condition to realize direct point to point personalized diagnosis, largely increases the potential possibility of preliminary disease detection hence improving personal health[9].

Potentiometry and Amperometry are the two basic transduction mechanisms applied in electrochemical sensing. With the application of ion-sensitive electrodes connected with the following potentiometric readout circuits, it is possible to detect in biofluid including potassium, sodium as well as PH. As for the detection of small biomolecules such as glucose, cholesterol, lactate, amperometric sensors are widely used.

In comparison with blood and interstitial fluids which are commonly used in medical diagnostic, salivary PH is a non-invasive and quick approach to monitor body condition and reflect the relevance of periodontal diseases as the fact that biomolecules in saliva show a high correlation to serum [10][11]. Therefore, it contains a large research value on saliva analysis providing enabling real-time measurement. Through a miniature intraoral wearable system integrated with an electrochemical sensor, continuous measurement of biomarkers over certain periods can be achieved while the intervention of other biomolecules and variability of the environment affect the obtained results to a different extent[12].As salivary pH reflects the health state with its inherent circadian rhythm, electrochemical biomolecule sensors provide real-time readings calibrated with pH value, to realize which, concurrent measurements of potentiometric and amperometric sensing approach is used for co-analysis based on monitoring various analytes [13][14].

In addition, pros and cons of potentiometry and amperometry techniques result from their intrinsic difference.[15].The amperometric method enables faster measuring of glucose while the potentiometry provides a wider range of detection. The input-output characteristics of both techniques applied sensors also differ in that the former one has a linear response to the input and the latter one is logarithmic. Integration of both approaches utilized in reconfigured circuits is capable of combining advantages of either technique hence resulting in more versatile analysis of biofluid. Some investigation on those topology mixing up potentiometry and amperometry in different modes has been demonstrated for desired feasibility even though performed in different time slots.

## 1.2 objectives

To achieve simultaneous potentiometric and amperometric measurement with the capability of detection of the instantaneous change in pH, Dual Amperometric and Potentiometric Power Efficient Instrumentation (DAPPER) is introduced as a system for accurate calibration and reliable analysis[16]. Based on DAPPER, this project aims to design a novel front-end read-

out circuits system that is used in portable biosensors, decoding current and voltage signals generated on the biofluid-immersed electrodes into the digital domain information, providing simplicity and accuracy for wireless data transmission through analog signal processing. The improved sensor combines amperometric and potentiometric signals into single-channel output with improved power consumption and better linearity, interfaced with wireless platforms at the backend.

## 1.3 Thesis Outline

Chapter 2 presents the background knowledge necessary to understand the electrochemical biosensors as well as its principle behind, the basic structures of potentiostats and the CMOS instrumentational readout techniques including Amperometry and potentiometry.

Chapter 3 presents the initial design of the concurrent amperometric and potentiometric sensor with its basic structures, working principles and the limitations.

Chapter 4 introduces the novel way to implements the read out methods by using other types of topologies to overcome the existing flaws on DAPPER sensing circuits. The systematic simulations are carried out to present improved results.

Chapter 5 presents a conclusion including the general summary of the project, the improvements on the DAPPER biosensor and the non-idealities. Future work is also discussed.

# Chapter 2

## Background Theory

### 2.1 Biosensor

As the evolution of the biochemical sensing process facilitates improved healthcare and research applications, the global sales of biosensors are estimated to achieve \$20 billion by 2020[17]. Electrochemical sensing techniques develop as the most trending approach amongst biosensing technologies due to their wide application in measuring biological analytes levels then transduces the intangible bio-information into electronic signals for easier transmission and processing[18][19]. Electrochemical biosensors enable detection of a large variety of biological recognition events such as enzyme reaction[20] or elements such as hybridized DNA[21], neuron tissue[22], and bacteria[23] or biofluids such as blood, sweat, and urine; There are many advantages of utilizing electrochemical sensors since its time efficiency, expense saving, label-free detection. In particular, there is no necessity for affinity binding hence allowing consecutive real-time measurement. Furthermore, electrochemical sensors are widely used for miniaturization such as wearable devices[24]. Optical biosensors translate the light into electronic signal based on the fact that properties of light are susceptible to biochemical reaction such as luminescence, fluorescence absorbance, etc, hence reflecting the activity of analyte. In comparison with optical counterparts, electrochemical sensors have better immunity to the interference of environmental variables[18].

The rapid progress on the development of microelectronics over the past decades has stimulated a large advance of complementary metal oxide semiconductor (CMOS) integrated circuits technology, permitting setting up solid but economic electronic platforms perfectly fitted for implementation of electrochemical instrumentation. The growth of CMOS-matched micro-electrodes enables establishing miniaturized biosensors on silicon chips. Unlike bulky traditional sensors and instrumental equipment, CMOS biosensors realize smaller scale, lower power consumption and are much less expensive[25]. Additionally, high-density CMOS biosensor arrays formed innovative platforms with improved detection such as DNA testing. [19] Over the recent decade, numerous different types of CMOS electrochemical circuits are designed which provide variable instrumentation features and performance characteristics[26].

## **2.2 Electrochemical Biosensor techniques**

An electrochemical biosensor normally constitutes four major components including analyte, bio-interface, transducer, and instrumentation, depicted in Fig.2.1. The analytes are the aimed biomolecules to be measured for instance glucose, protein, nucleic acid, etc. The bio-interface also name as bio-recognition element enables selectively identifying the targeted analytes. The transducer extracts physical information to describe the interactions between the analyte and bio-interface by conveying electric signals in form of voltage or current such as chemical reactions induced by ionization. The instrumentation normally consists of complex electronic circuitry which receives and processes the electronic signals transmitted from the transducer. The immersing electrolyte solution forms a liquid environment impart biological activity of analytes and the capability of analyte's movement to the transducer. .

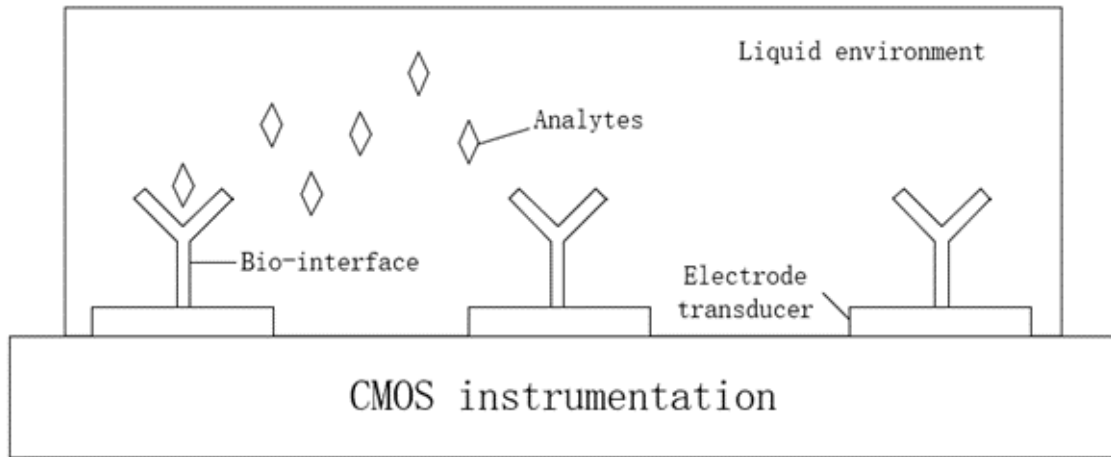


Figure 2.1: Electrochemical biosensor structure

A large variety of electrochemical techniques are utilized in characterizing biosensors or measuring characteristic responses with external stimulus or internal biochemical reactions. Many widely applied electrochemical techniques such as potentiometry, amperometry, voltammetry, and impedance spectroscopy are introduced and classified based on their sensing mechanism, electrode materials, and interface reactions [27].

### 2.2.1 Potentiometric biosensor

Potentiometric biosensors measure the concentration of analytes by inducing constant voltage potential difference when zero current conducting through electrodes. Additionally, an adjustable DC current can be applied to electrodes generating the linear response at the sensing circuit which is positively proportional to the density of targets[28] shown in Fig.2.2. Potentiometric biosensor dominates in commercial application and research due to their simplicity and low cost to build up whereas the selectivity is not desirable enough in some particular circumstance[29]. Apart from the sensor direct response current, the current response of the potentiometric biosensor is also highly associated with the electrode double layer charging current which is physically functional as a double layer capacitor following most electrochemical sensor models. Due to the large difficulty to eliminate the influence of parasitic charging current by simple filtering, the selectivity of a potentiometric biosensor is restricted[30]. Among many

potentiometric biosensors, redox-potential biosensors are popular in utilization in glucose and DNA detection dependent on the redox reaction of biomolecules[31].

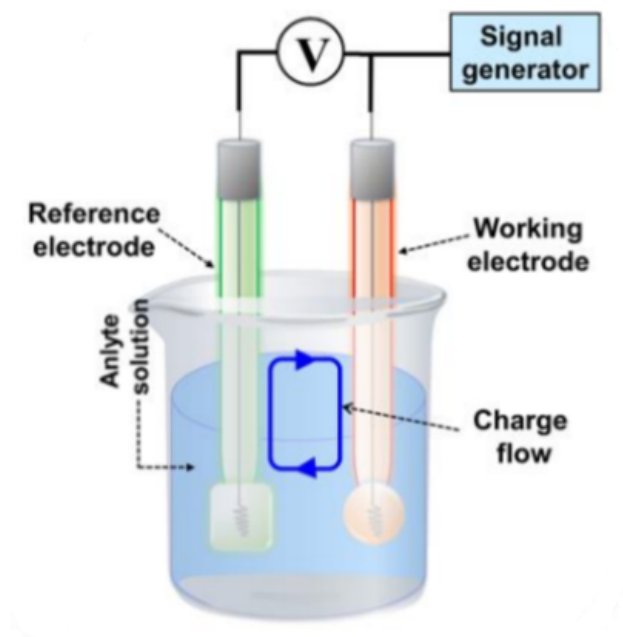


Figure 2.2: Potentiometric measurement [1]

### 2.2.2 Amperometric biosensor

In traditional amperometric biosensors shown in Fig.2.3, a DC response current is produced and measured when there is a controlled DC voltage applied. The response current is fundamentally proportional to the density of analyte of interest and subjective to oxidation and reduction of biomolecules through the sensing process. When controlled DC voltage is applied between electrodes to provide electronic energy impetus, the oxidation/reduction events are activated across the interface between electrode and electrolyte leading to the biorecognition process. Voltammetry normally refers to the DC current response obtained from varied DC voltage stimulus such as a ramp signal.

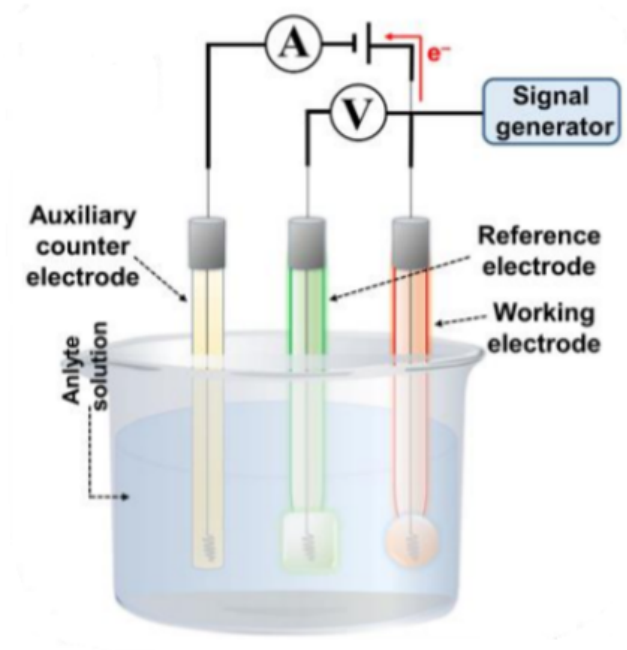


Figure 2.3: Amperometric measurement [1]

### 2.2.3 Impedimetric biosensor

Apart from two commonly employed biosensors to measure DC response, impedimetric biosensors are introduced to measure the AC electrical impedance across electrode-electrolyte interface when reaching equilibrium as the overall structure of the electrode-electrolyte interface is modeled as a combination of resistance and capacitance[32]. Unlike applying relatively large voltage stimulus in either potentiometric or amperometric biosensors, impedimetric biosensors simply require a small sinusoidal voltage signal (usually 5-10 mV in amplitude) as driving force with the controlled frequency with negligible interference on layers then measures the generated current, based on which the phase and amplitude can be extracted to gain the impedance information thus reflecting the occurring biorecognition process. Electrochemical impedance spectroscopy (EIS) is one of the impedimetric techniques widely employed in many applications including measuring CD4(+) cell density [33], detecting heavy metal ions [34] and receptive bilayers monitoring [35].

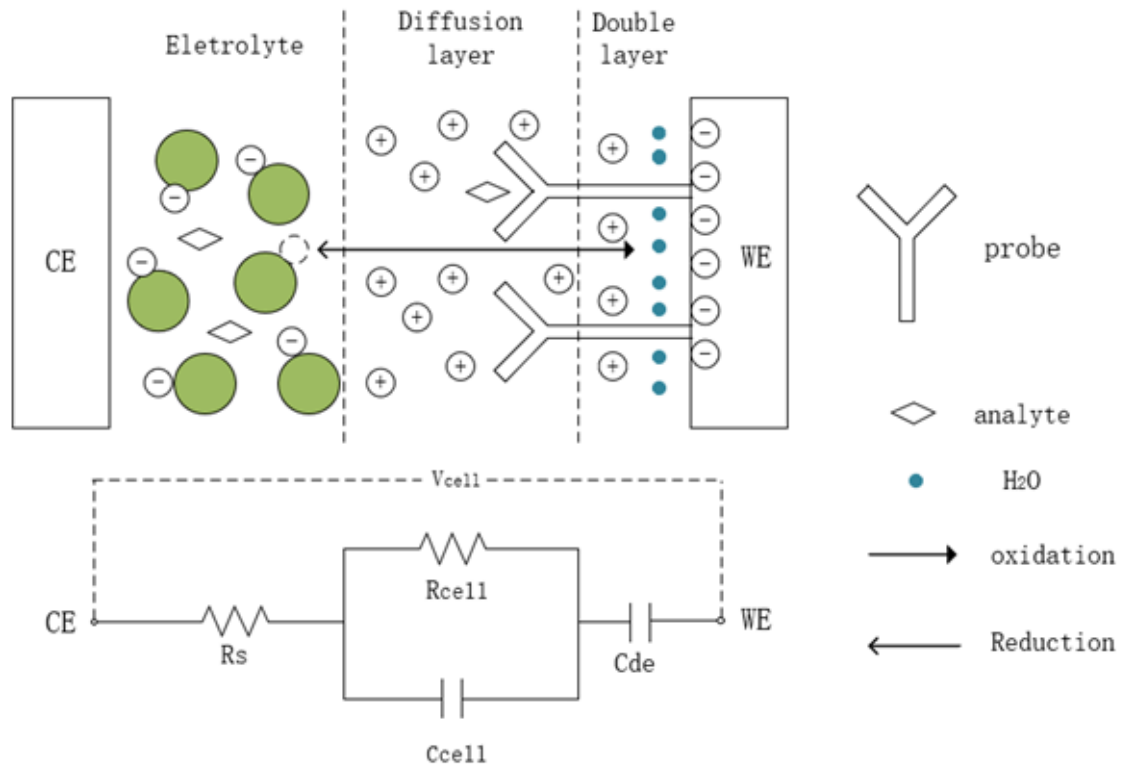


Figure 2.4: The charge profile of the electrode-electrolyte interface [2]

The charge profile of the electrode-electrolyte interface is shown in Fig.2.4 as well as the equivalent circuit model. According to the model,  $R_s$  represents the resistance of electrolyte solution between the working electrode and counter electrode. The  $C_{cell}$  represents the capacitance of diffusion layer.  $C_{de}$  represents the capacitance of double layer at working electrode interface.  $R_{cell}$  represents the resistance of charge transfer at the working electrode interface. The double-layer is formed of two layers, one layer between dissolved positive ions and water molecules and another one between water molecules and ions at the working electrode interface. Biochemical probes integrated with working electrodes in diffusion layer are used to detect analytes.

#### 2.2.4 Ion-sensitive Field Effect Transistor Biosensor

From an instrumentation point of view, ion-sensitive field-effect transistor biosensor (ISFET) measure ion concentration with a similar working principle of metal-oxide-semiconductor field-

effect transistors (MOSFET). In MOSFET, the current induced between drain and source is positively proportional to the voltage applied to the gate. The ISFET is reconfigured MOSFET with gate terminal modified as molecular acceptors or targeted ion filtering membranes for the substance of interest shown in Fig.2.5. The electric voltage changes induced by bioreaction at the gate oxide layer at the gate terminal leads to depletion or accumulation of carriers[3]. As the induced current through the channel is subjective to the electric field produced by reactions during biorecognition events which is similar to apply voltage to the gate terminal, ISFET can be utilized as a satisfying biosensor with good performance to monitor ion concentration such as pH, enzyme[36], and DNA[37], etc.

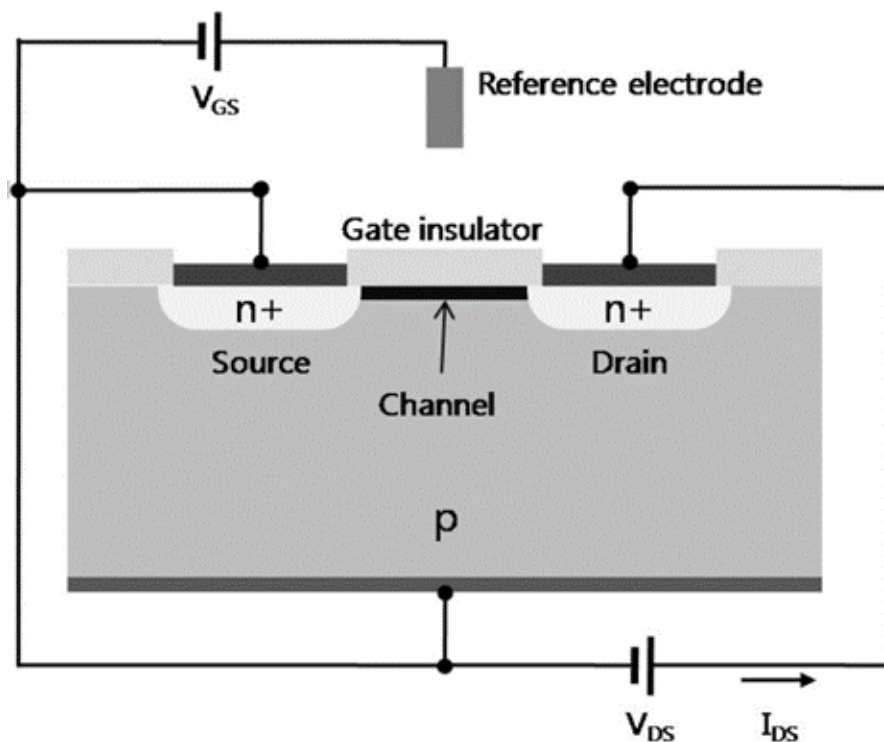


Figure 2.5: Structure of ISFET. It consists of source, drain, gate insulator, and reference electrode. [3]

## 2.3 Electrode transducer

As it is mentioned above, except ion-sensitive field-effect transistor biosensor, the electrode transducer is of utmost importance to potentiometric and amperometric biosensors which enable translating biorecognition process to electrical information. The electrodes are semicon-

ductive and interfaced with electrolyte solution classified as working, reference, and counter (auxiliary). Working electrode is designated to pass current to other analytes to evoke targeted electrochemical reactions. Reference electrode, as its name suggests, hold a constant potential as a reference without current flowing through. Counter electrode is introduced to completes the current path in three electrodes system. Working electrodes where electrochemical reactions of interest occur and counter electrodes playing a role as the other half of the cell together consist up to two electrodes configuration. The controlled variable voltage is applied between two electrodes externally resulting in a current response at either electrode. The counter electrode functions as not only a reference potential maintainer without being affected by current flowing through but also a current source/sink, which is key to two-electrode system. As is shown in Fig.2.6, the applied voltage  $E_A$  consists of constant counter electrode potential ( $e_C$ ), working electrode potential ( $e_W$ ) as well as the voltage drop across the solution ( $iR_s$ ). For better control of  $e_W$ , there needs to be an additional electrode working as either reference or current path to alleviate the tasks of the counter electrode, to overcome the influence of  $iR_s$  as the resistance of solution works as potential divider subjected to the environmental variable, which is unremovable but error-causing.

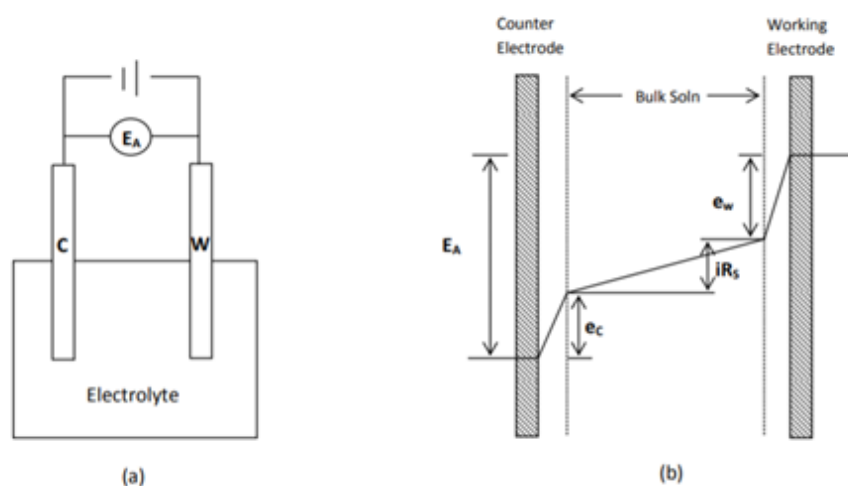


Figure 2.6: Simple schematic of two electrode configuration. [4]

By adding a reference electrode to the system shown in Fig.2.7, the counter electrode acts as a current path while the reference electrode is responsible for working electrode potential control and reference potential offer regardless of current density, according to which, the error

caused by a voltage drop across the ion path within solution can be eliminated. However, there is a minor voltage drop between the reference electrode and the working electrode ( $iR_u$ ) negligibly influencing the measured results as illustrated in the figure. Introduction of reference electrode set up much more stable system to maintain unchanged reference potential and compensation for the voltage drop across the solution, which is widely used in electrochemical biosensors particularly for amperometric techniques where larger response currents are required. As for the counter electrode, the current feedthrough balances the current generated at the working electrode causing the extreme potentials to be reached at the counter electrode[38].

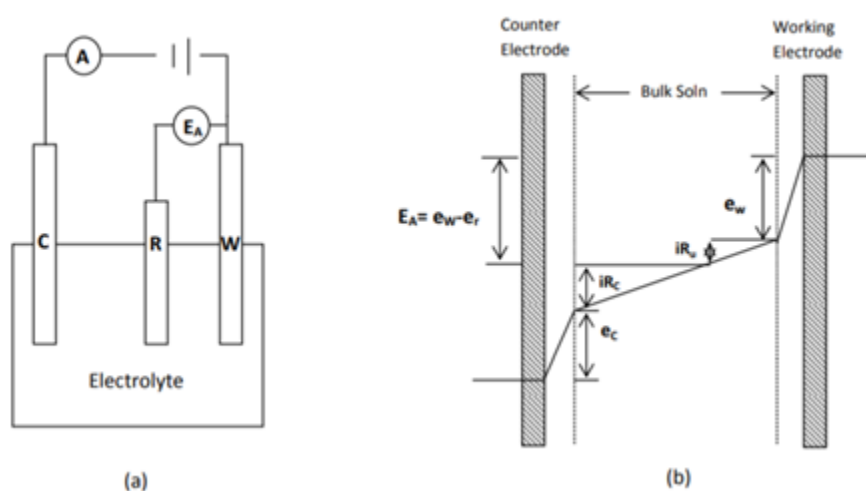


Figure 2.7: Simple schematic of three electrode configuration. [4]

## 2.4 CMOS instrumentation for amperometric and potentiometric biosensors

As is mentioned above, the electrodes are employed as an electrochemical platform where the biorecognition process takes place and is decoded into electrical information such as current and voltage response. The instrumentation does not only measure the electrical domain signals but also supply biasing signal to inject enough energy to promote biochemical reactions. According to the biosensor applications over recent years, CMOS technology is ubiquitously utilized for its robust performance and low cost.

Potentiometric biosensors circuits measure the potential difference between electrodes by implementing voltage follower circuit topology shown in Fig.2.8 at the first stage connecting the input of operational amplifier of high impedance to the electrodes, forming perfect electrical isolation of output to the input source. Therefore, loading effects are largely reduced as very little current is feed through the input terminal from the signal source. The second stage of the circuit is made of a buffered differential amplifier with three resistors connecting two buffer circuits. The voltage difference between reference electrode(RE) and working electrode(WE) are identically replicated as the voltage drop across the  $R_{gain}$  resistor. The following regular differential amplifier amplifies the voltage drop as the factor of unity. The overall gain is mainly determined by the value of  $R_{gain}$  resistor which is adjustable. In addition, there are some advantages of this topology including high input impedance, high common-mode rejection ratio (CMRR), and good noise immunity[39].

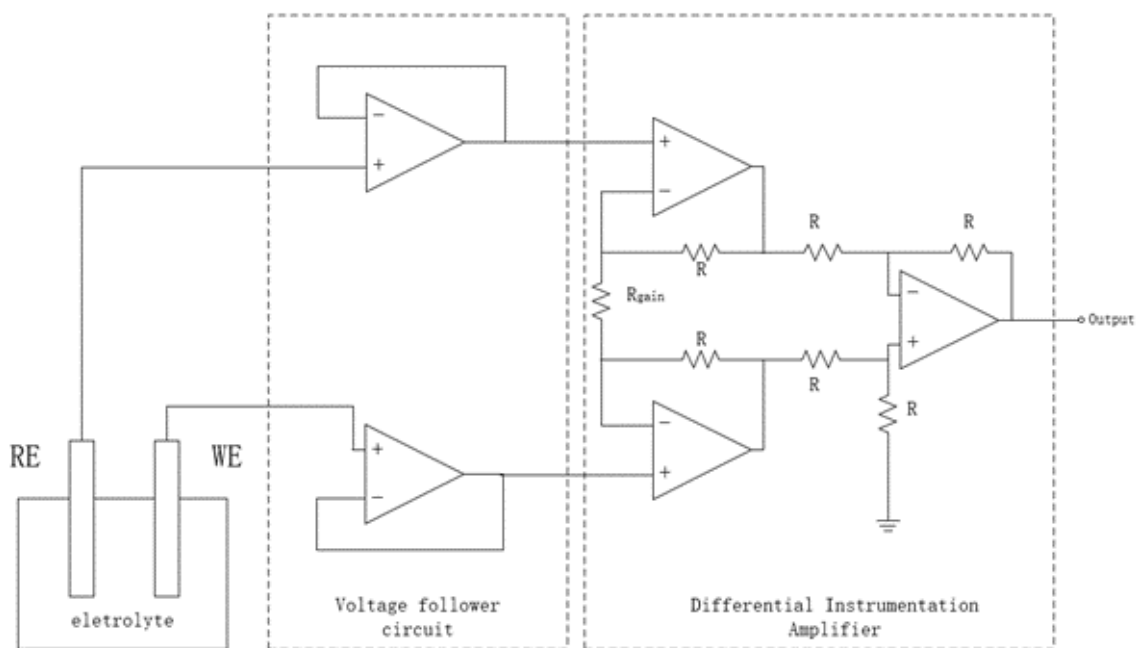


Figure 2.8: Instrumentation circuit in potentiometry.

CMOS electrochemical instrumentation for amperometric biosensors can be generalized as several components, illustrated in Fig.2.9 : signal generator, potentiostat, readout circuit, and signal processing. The built-in low noise signal generator produces desired driving signals including DC, pulse, ramp, and triangle waveform. The potentiostat usually contains an opera-

tional amplifier to supply potential bias at electrodes. The electrical signal is then generated as the bio-recognition process occurs at the electrode-electrolyte interface. The read-out circuits detect and amplify current response for further signal enhancement at the signal processing stage.

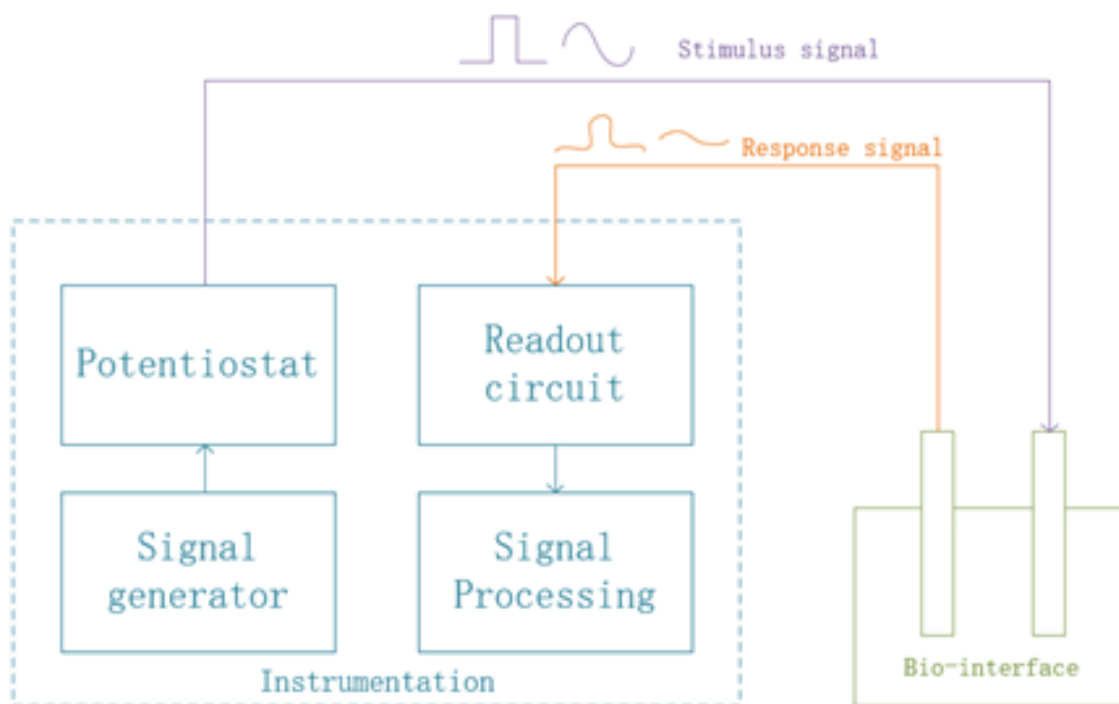


Figure 2.9: The structure of the instrumentation for electrochemical biosensors.

### 2.4.1 Potentiostat

Potentiostat is the block of biasing circuit which provides accurate constant potential at the electrode-electrolyte interface to trigger redox reaction of analyte during the recognition process. The simplest potentiostat consists of a single operational amplifier used in a two-electrode amperometric electrochemical system. As the three electrodes system is more superior to the two electrodes system[40], for which most CMOS potentiostats in modern industry are designed, usually configured by setting one of the electrodes to be ground reference[41]. There are two common configurations called grounded-WE and grounded-CE which function as the same in potentiostat. Grounded-WE shown in Fig.2.10, as its name suggests, connect the working electrode to the analog ground while the other two electrodes consist up as a negative feedback

loop with an operational amplifier with external voltage applied at the non-negative input terminal and output connected to the counter electrode, driving the negative input terminal linked with reference electrode to reach at the same potential as external stimulus voltage since reference electrode and the counter electrode are electrical connected with electrolyte solution represented as a resistor. Then the potential of the reference electrode and counter electrode reaches the desired external voltage value, forming a constant potential gap between the reference electrode and working electrode which can evoke electrochemical reaction at the electrode-electrolyte interface. Therefore, the sensing current is generated and fed through the working electrode, measured by the following readout circuit.

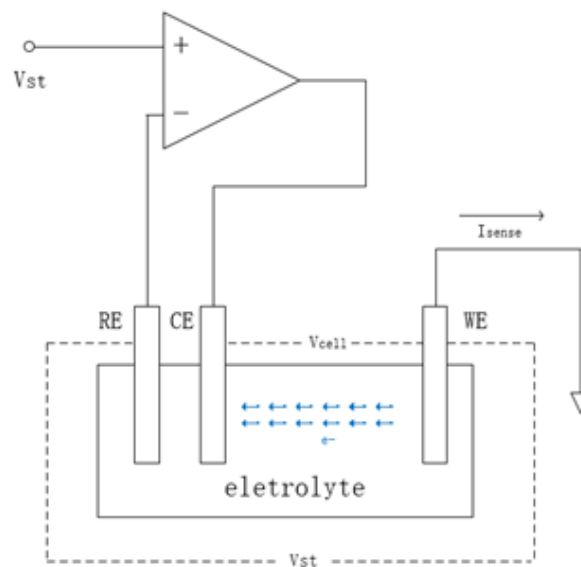


Figure 2.10: Three-electrode potentiostat with the grounded-WE structure.

Comparatively, the grounded-CE potentiostat is more complex and less commonly used with a counter electrode linked to the ground[42]. As the potential between the working electrode and the reference electrode is required to be constant at an externally supplied voltage and unvaried regardless of the variation of potential at the working electrode and reference electrode guaranteeing continuous electrochemical reaction. The standard three electrodes potentiostat system configuration is shown in Fig.2.11 where three operational amplifiers are employed to force the potential at the working electrode to be the sum of stimulus voltage and the varied reference voltage. Thus, the potential gap between the working electrode and the reference

electrode is maintained at the targeted stimulus voltage.

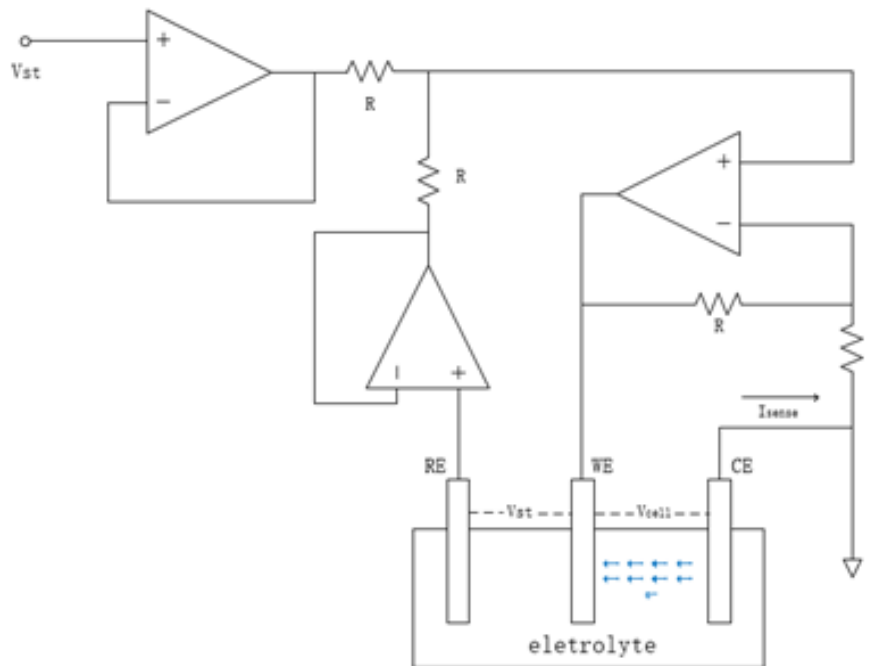


Figure 2.11: Three-electrode potentiostat with the grounded-CE structure.

## 2.4.2 Readout circuitry

### DC voltage readout circuitry

As is discussed in the instrumentation section, the bio-signal induced by stimulus supplied by potentiostat is translated to electrical domain signal at bio-interface then captured by the readout circuits. The voltage response in potentiometric biosensor can be processed to be converted to a current response with designed voltage to current topology then shares the same circuitry with amperometric biosensor, which simply reduces the complexity and tends to be modularized. Many potentiometric biosensors are implementing voltage-controlled oscillator (VCO) which maps the voltage signal into frequency as shown in Fig.2.12 However, VCO inherently contains the voltage to the current converter as the first stage and the current-driven oscillator as the following stage. Thus, the readout circuits in potentiometric biosensor intrinsically share the same structure with the readout circuit applied in amperometric biosensor with difference performance required which is discussed later.

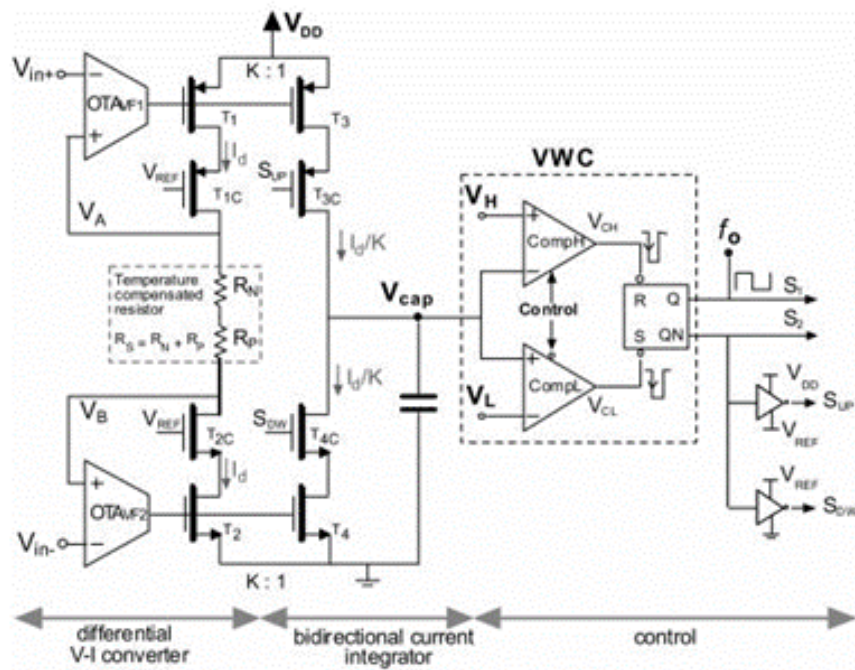


Figure 2.12: The schematic of DC voltage readout circuit[5]

### DC current readout circuitry

From instrumentation's perspective, the types of current readout circuits are divided into two DC and AC determined by the current response generated at bio-interface. This thesis mainly focuses on DC current readout circuits. Normally the amperometric readout circuit is qualified in large dynamic range, high noise immunity, bi-direction measurement as well as desirable bandwidth. Based on a large number of amperometric biosensors applications with customized functionality and characteristics coming up over decades as modern microelectronics advances, the mainstream configurations can be classified as resistive feedback, capacitive feedback transimpedance amplifier(TIA), and current conveyor.

### Resistive feedback current readout circuits

The sensing current from the electrode can be simply measured in form of voltage through a resistor based on ohm's law shown in Fig.2.13. To configure the resistor as a constant voltage signal generator with ideally minor output impedance and no current reduced at following

circuits, an operational amplifier with a resistor as feedback is applied to convert the current response to voltage domain signal.

$$V_{out} = I_{sense} R_{feedback} \quad (2.1)$$

where,

$V_{out}$ : the output voltage of operational amplifier.

$I_{sense}$ : Sensing current from the electrode.

$R_{feedback}$ : feedback resistance.

$V_{out}$  represents the output voltage of the operational amplifier and  $R_{feedback}$  represents the feedback resistor. As the value of the feedback resistor is adjustable, the output swing of this configuration can be arbitrarily set. The current input-referred noise is represented as:

$$i_n^2 = \frac{4kT}{R_{feedback}} \quad (2.2)$$

where,

$i_n$ : The current input-referred noise.

$k$ : the Boltzman constant.

$T$ : the environmental temperature.

$R_{feedback}$ : feedback resistance.

To lower the current input-referred noise, the feedback resistor needs to be large. Nevertheless, the resistor is also restricted to the area limitation on the chip and undesirable for large bandwidth applications. In other words, the resistive feedback current readout circuit is not an ideal structure to build up a powerful platform with low noise and high bandwidth performance in modern biosensor applications even if having better noise performance in the high bandwidth than the capacitive counterpart[43].

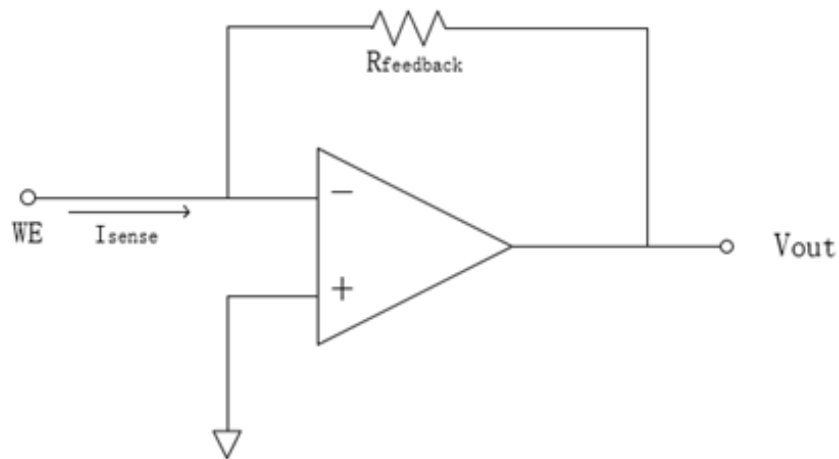


Figure 2.13: Resistive feedback current readout circuit

### Capacitive Feedback Current readout circuit

For better readout resolution, the capacitive feedback current readout circuit replaces the resistive feedback current readout circuit as the resistor induces large thermal noise and occupies a large area. Capacitive feedback current readout circuit has good noise immunity in low bandwidth application which is shown in the Fig.2.14

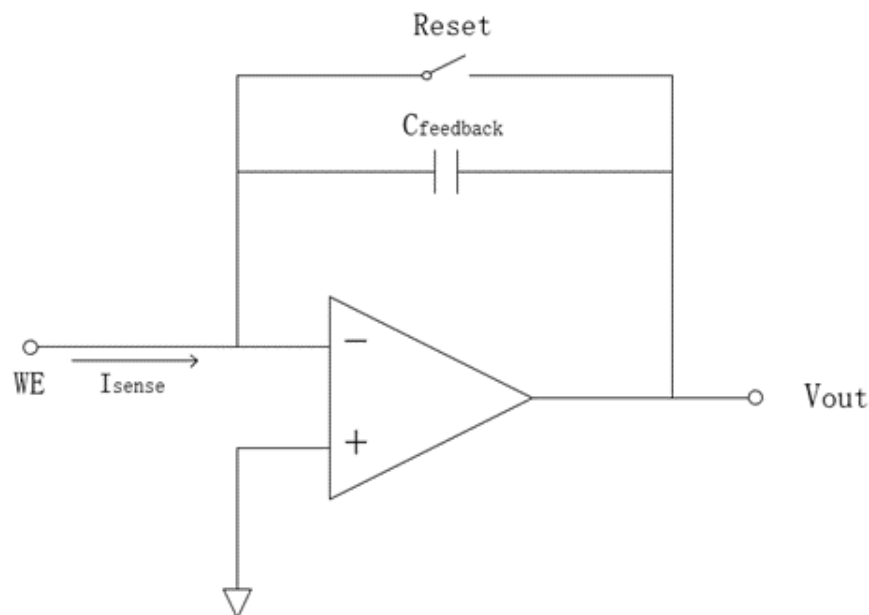


Figure 2.14: Capacitive feedback current readout circuit

where operational amplifier and capacitor forms an integrator with periodic on/off switch to realize the conversion of current to voltage. When injecting DC current into the integrator, the charge accumulates at the capacitor over period T leaving output voltage represented as

$$V_{out} = \frac{1}{C_{feedback}} \int_0^T I_{sense} dt \quad (2.3)$$

where,

$V_{out}$ : the output voltage of operational amplifier.

$I_{sense}$ : Sensing current from the electrode.

T: the period of integration.

$C_{feedback}$ : feedback capacitance.

The output voltage is continuously an increasing ramp signal if the sensing current is constant. When reaching a certain level, the switch is closed forming a short circuit of capacitor then discharging the capacitor until the switch is reopened back to integration mode. Although switched capacitor technology largely reduces the overall noise compared with resistive counterpart, some noise sources influence the resolution of the readout circuit classified as channel charge injection, clock feedthrough, sampled noise, and leakage current, generally summarized as input offset errors that can be overcome by applying cancellation techniques. Autozeroing is a good offset removal technique to subtract constant noise by highly filtering low-frequency random noise such as flicker noise which is considerable in the current readout circuit and reducing it at low frequency at the cost of increased wide-band noise due to aliasing. Correlation double sampling (CDS) improves the autozeroing process with sample and hold circuit, containing two sampling operations: sampling offset and noise and sampling the targeted signal and the instantaneous noise[44]. The noise and offset are removed based on subtraction from the output signal leading to a resulted signal with less offset and noise. The correlation double sampling also introduces double thermal noise as one of the drawbacks thus the amplifier needs to be specifically designed[25]. The example of correlation double sampling circuits is shown in the Fig.2.15. where the sampling is carried out by sets of switches controlled by two opposite

phase clock signals.

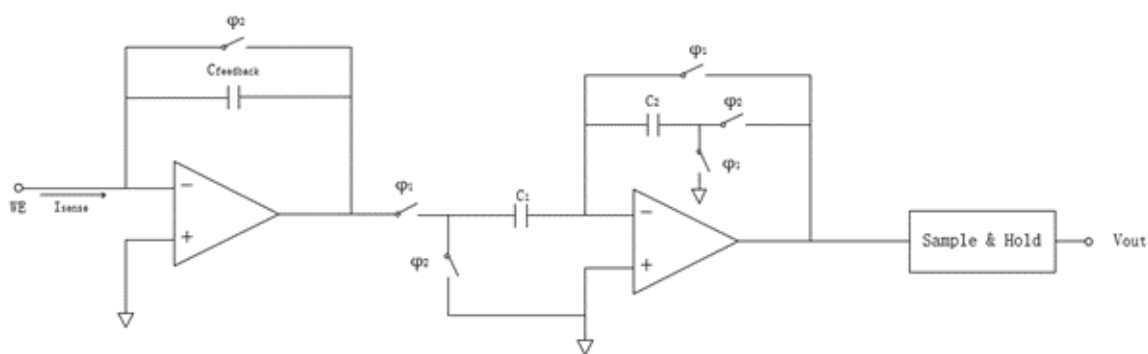


Figure 2.15: Structure of correlation double sampling circuit

### Current conveyer Current Readout Circuits

The current conveyer structure is widely used in amperometric biosensors by implementing a current-mode amplifier to reduce the noise and current mirrors to duplicate current with a specific ratio. The current conveyer structure is shown in Fig.2.16

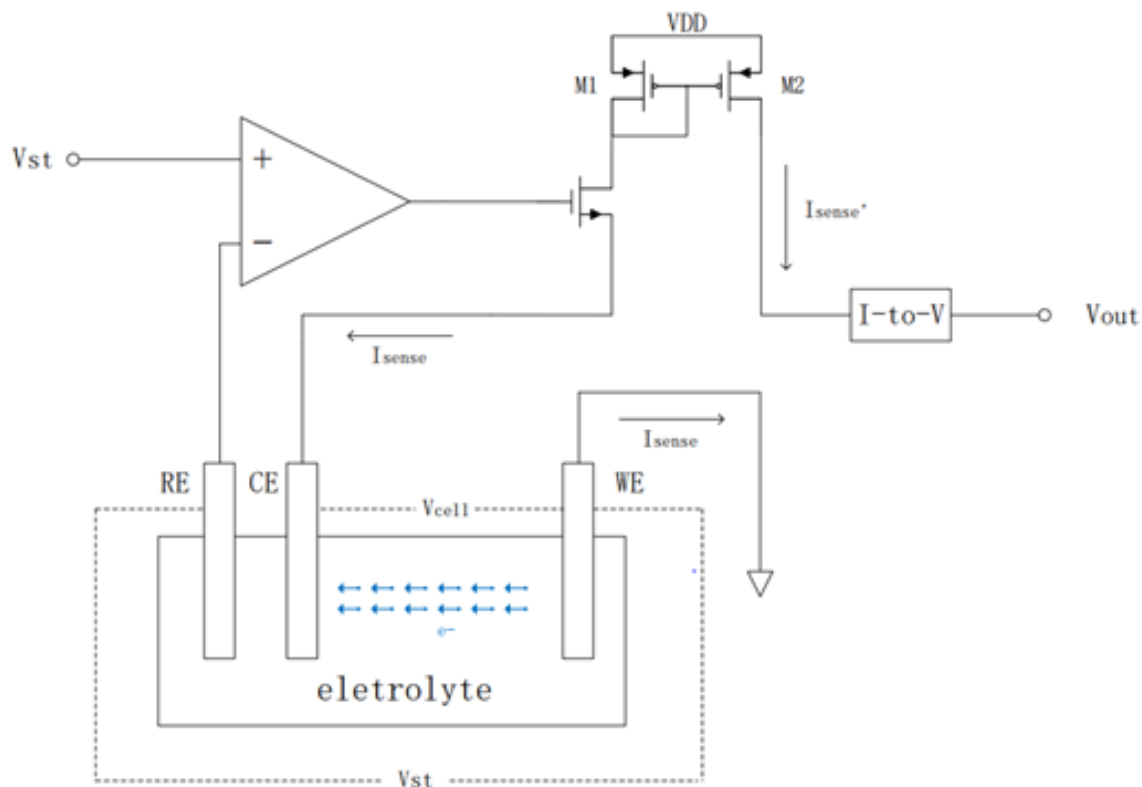


Figure 2.16: Structure of current conveyer circuit

As is introduced in the previous section, counter electrode, electrolyte and working electrode form a current route that the current is injected into the counter electrode. The current mirror works as a current source copying the current response through the function shown below and output to the following current to voltage circuits.

The current magnitude ratio is positively proportional to the dividend of aspect ratios of current mirror transistors. Compared with the capacitive feedback readout circuit, the current conveyor is much more area-efficient as there is no capacitor or resistor required while achieving decoupling and linear operation in the current domain[45]. Another advantage of applying the current conveyor structure is that sensing current can be amplified through the current mirror that there is no necessity to output large current for the operational amplifier, imparting very low power consumption to the overall system. To measure bi-directional current, the current sink needs to be added as shown in Fig.2.17. For better performance, the current mirror can be cascoded to increase the stability of the output current[46].

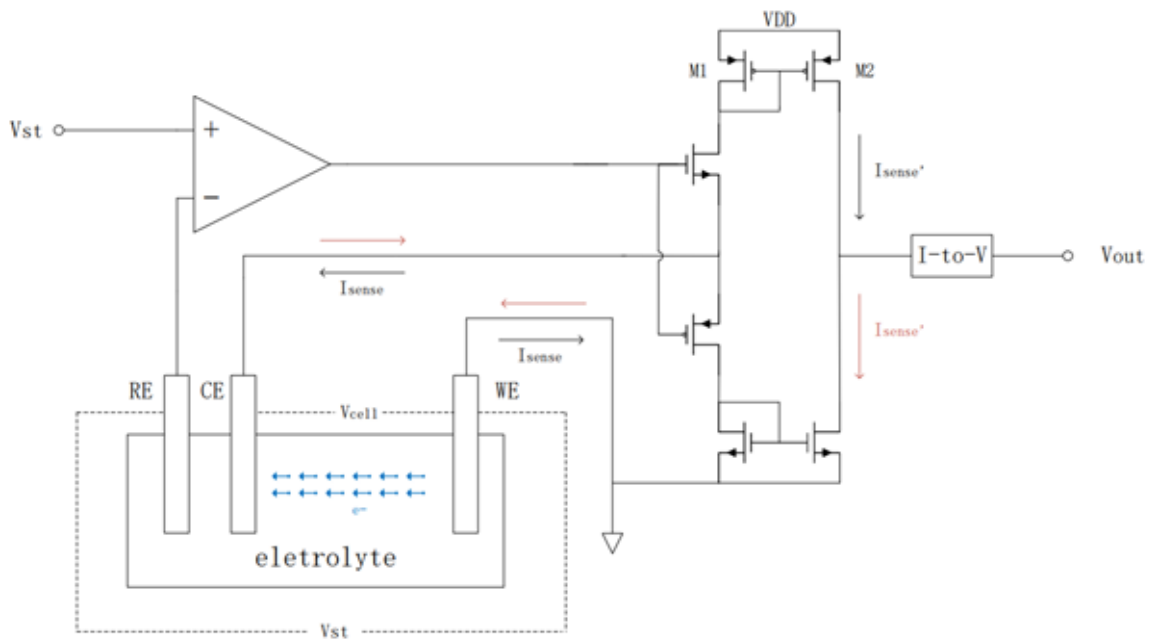


Figure 2.17: Structure of current conveyor circuit with current source/sink

## Digital processing of DC current readouts

As the electrical signal is successfully captured by the readout circuits, the most important step is to translate the analog signal into a digital signal which advances in accurate data transmission and analysis. The most common topology employed in amperometric biosensors is a customized analog-to-digital converter (ADC) classified in sigma-delta()ADC[47], successive approximation ADC[48] and integration ADC[49]. The example of hybrid ADC[50] with a simpler structure is shown in the Fig.2.18 mixed with the advantages of sigma-delta ( $\Sigma\Delta$ ) ADC with noise shaping and integration ADC, applied in high-performance instrumentation and measurement applications.

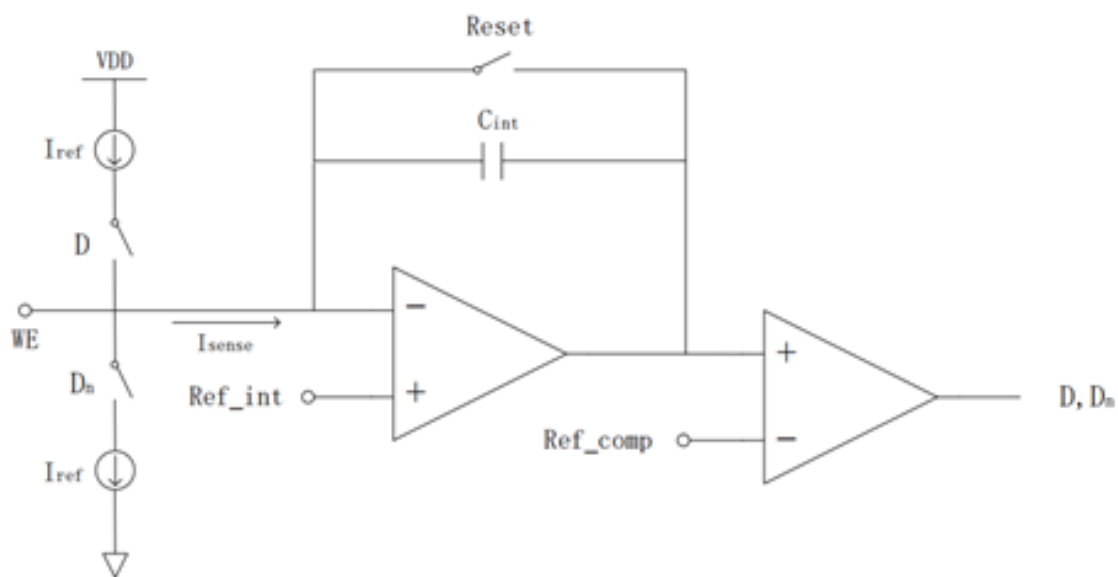


Figure 2.18: Structure of a first-order incremental current mode ADC circuit for amperometric sensing

First order sigma-delta  $\Sigma\Delta$  ADC is desirably powerful due to its high resolution and large detective range while featuring at small area and low power consumption. One typical application is shown in the Fig.2.19.

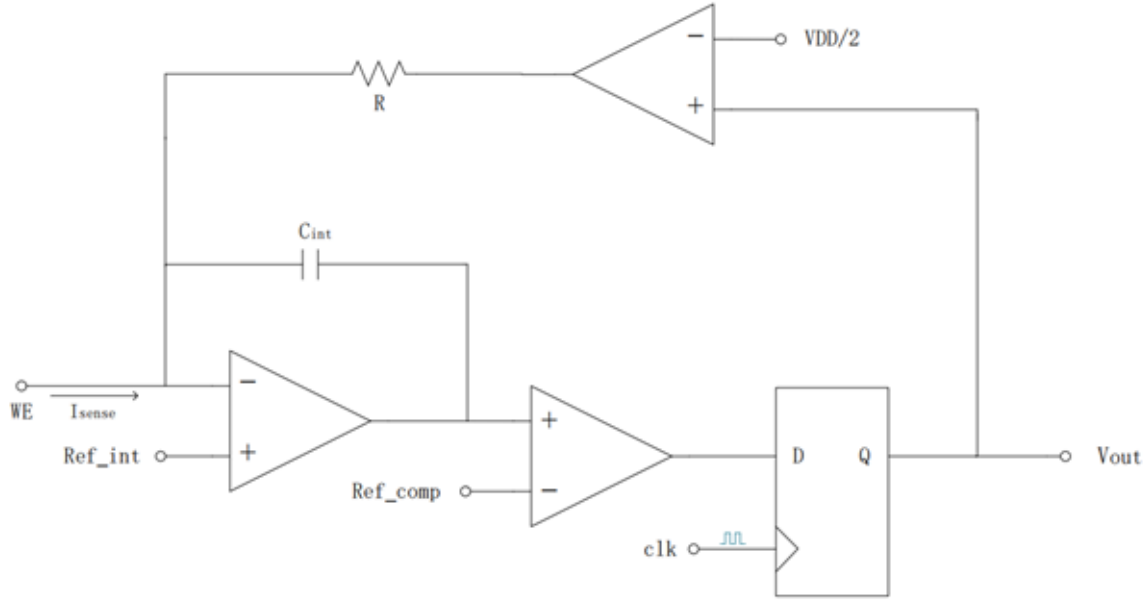


Figure 2.19: First-order incremental current mode  $\Sigma \Delta$  ADC circuit in application

The analog current signal is linked to the input of the integrator generating ramp voltage signal at the output of the integrator, then compared with the reference voltage at the negative terminal of the comparator which corresponds to 1-bit ADC, producing either digital high or low. The output of the comparator is fed through a D-type flip flop driven by a high-frequency clock signal then fed back to the input of the integrator through the second comparator at the top side referenced at half power supply. The final comparator acts more like a switch to flip over the output of the d-type flip flop then feedback to the integrator. When the integrator outputs voltage above the reference voltage, the first comparator will output a high signal to the D input of the flip-flop. As the clock signal rises up to a high level, the D flip flop captures the logic high level of the comparator output then output to the negative terminal of the amplifier of the second comparator. Since the logic high voltage is greater than the half power supply voltage, the second comparator outputs zero voltage to the integrator working as a constant current sink corresponding to current  $I_{ref}$ , forcing the capacitor to discharge until integrator outputs drop down below the reference voltage. The reference current  $I_{ref}$  is expressed as:

$$I_{ref} = \frac{V_{ref}}{R} \quad (2.4)$$

where,

$I_{ref}$ : reference current in two directions for capacitor charging and discharging.

$R$ : the resistor linked between the input channel of integrator and output of the comparator.

$V_{ref}$ : the reference potential at non-negative terminal of integrator..

$R$  is the resistor linked between the input channel of integrator and output of the comparator.

As  $R$  can be adjusted, the reference current can be manageable as desired. Normally the reference voltage is half power supply for simplicity, the magnitude of reference current is  $\frac{V_{DD}}{2R}$

The discharging current can be represented as:

$$I_{discharge} = \frac{V_{ref}}{R} - I_{sense} \quad (2.5)$$

where,

$I_{discharge}$ : capacitor discharging current.

$I_{ref}$ : reference current in two directions for capacitor charging and discharging.

$R$ : the resistor linked between the input channel of integrator and output of the comparator.

$V_{ref}$ : the reference potential at non-negative terminal of integrator..

If  $V_{ref}$  equals to half power supply, the discharge current equals to  $\frac{V_{DD}}{2R} - I_{sense}$

Based on previous analysis, the first comparator output low voltage as potential at the non-negative terminal is less than the reference voltage. When entering the next clock cycle, the logic low is renewed at the output of D flip-flop, inverting the second comparator output. Then the second comparator changes its role into the current source allowing the capacitor to start to charge and the output of the integrator ramping up.

That is how the signal-delta concept is expressed through topology. The integrator sums ( $\Sigma$ ) the comparator's output with the sensing current. The first comparator detects the difference as delta ( $\Delta$ ) between integrator output and the reference voltage. The output result would be a series of bitstreams similar to a clock signal. If no sensing current injection, the digital output is formed as:

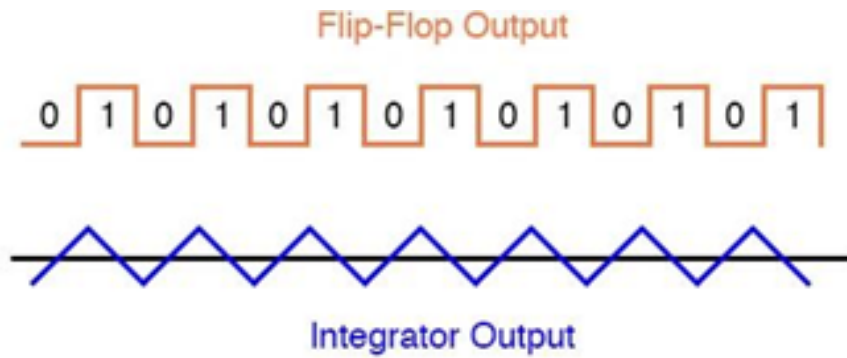


Figure 2.20: Output waveform of flip flop and integrator without input current [6]

Based on the formula shown before, if the reference voltage is half the power supply, the charging current is equivalent to the discharging current which is  $\frac{V_{DD}}{2R}$ . As the charging and discharging are finished within one clock cycle, any charging and discharging speed up simultaneously will not be detected and reflected from results. Therefore, the sensing current injected breaks the equilibrium balance by slowing down discharging speed and increasing the charging speed if its direction is positive. The resulted waveform is shown as:

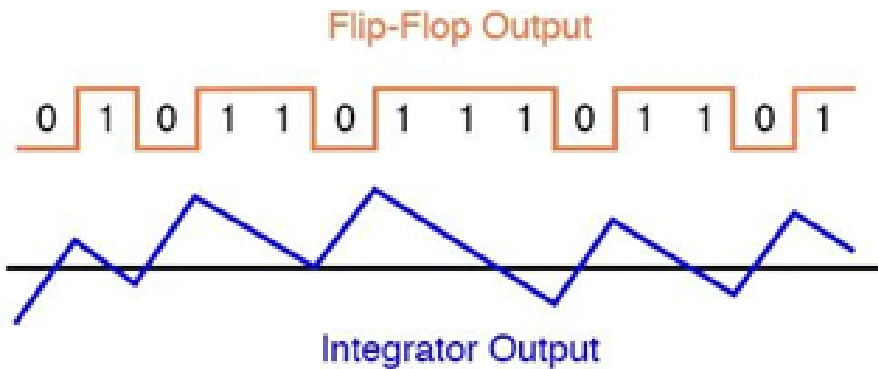


Figure 2.21: Output waveform of flip flop and integrator with input current [6]

The duration of charging and discharging are not explicit to figure out which indicates that an additional counter is demanded to count up the total number of logic 1 within a certain limited time range. Then the sensing current can be obtained by specific extraction of acquired digital information. As the sensing current is larger, the ratio of time of charging and discharging gets large leading to more logic 1 are output and counted. In other words, the magnitude of sensing current is positively relevant to the counter results but not an exact linear relationship.

# Chapter 3

## Initial design of potentiometry and Amperometry

### 3.1 Overall structure

THE overall structure of the concurrent potentiometric and amperometric circuit system is depicted as Fig.3.1.

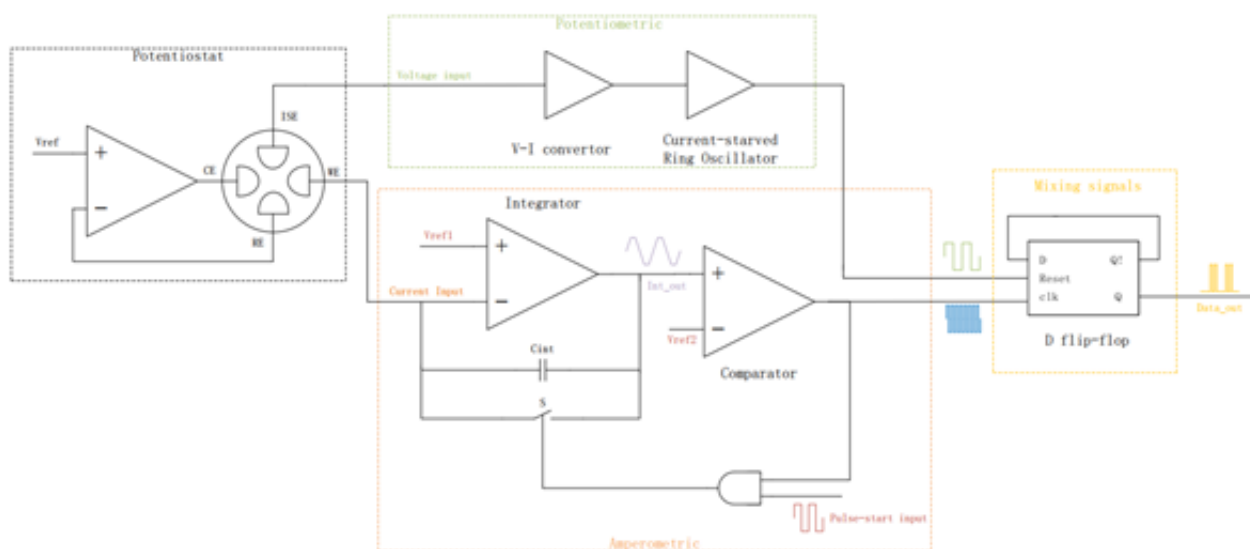


Figure 3.1: The overall structure of proposed sensor

The entire system consists of four blocks, potentiostat, potentiometric sensing, ampero-

metric sensing, and signal mixing, from detecting generated bio-signal to finally outputting a single-channel digital signal with varied frequency, conveying concentrations of targeted analytes in the oral environment.

The proposed potentiostat uses a shared reference electrode structure translating bio-signal into DC response from working electrode and DC voltage response from Ion sensitive electrode without cross-interference. There is an open-loop amplifier with external reference voltage supplied, forcing potential at the counter electrode and reference electrode rising to reference voltage.

Potentiometric measuring circuit constitutes a voltage-controlled oscillator that converts the magnitude of DC input voltage to the frequency of square wave with linear relationship, divided into 2 steps. The first step is to use the current conveyor structure to transduce the magnitude of voltage into the magnitude of current proportionally. Then the current-driven oscillator called the current-starved ring oscillator generates a square wave of which frequency is a linear response to current. Depending on two steps, linear conversion from voltage to frequency at low power consumption is achieved.

Comparatively, Amperometric processing implements another current-driven oscillator which has a greater detective range but is more complex. Modified first-order incremental sigma delta ( $\Sigma$ ) ADC remains original integrator ( $\Sigma$ ) and comparator ( $\Sigma$ ) but replaces the discharging current source with reset switch which is controlled by the feedback of output of the comparator. The output voltage of the integrator oscillates in form of triangular form between two different levels of reference voltage which are applied to the integrator and comparator respectively. Then the comparator transforms the triangle signal to a square wave with an unbalanced duty ratio.

A D-type flip flop(DFF) combines the output of amperometry and potentiometry with one bit counter configuration by short connecting D and Qnot. The reset port is connected with low-frequency potentiometric output while the clock port is linked to high-frequency amperometric output, based on which, a high-frequency square wave of half duty ratio with periodic 'on' is achieved and output as final data.

## 3.2 potentiostat with shared reference electrodes

As is mentioned in the background section of potentiometry and amperometry, potentiometric biosensors are used to implement a 2 electrodes system that consists of sensing and reference electrodes to capture electrochemical signals generated through biochemical reactions. Ion sensitive electrode (ISE) is employed as a sensing electrode where targeted hydro ions are received. When those positive ions gather around the metal oxide made electrodes such as Iridium oxide pH electrode[51].

the equilibrium is formed contributing to a constant potential difference between the ion-sensitive electrode and reference electrode. For example, Iridium oxide acts as a film to filter out other biomolecules except for H<sup>+</sup> ions. By applying a high impedance voltmeter between ISE and RE, the density of hydro ions represented by junctional potential relative to reference voltage is measured without current flowing through electrodes guaranteeing stable equilibrium. However, the equilibrium can be unbalanced with the occurrence of random potential disturbance while current is induced through electrode according to Faradays' law [52].

Based on the three electrodes' potentiostat structure, classical amperometric measurement is applied in this system. A voltage follower with external stimulus voltage force the reference electrode and counter electrode to reach a certain reference voltage level. As the potential gap between the working electrode and reference electrode is created, the diffusion of ions of interest takes place with moving direction towards the working electrode, triggering redox reaction at the electrode surface [53].

The side products of the redox reaction diffuse in opposite directions away from the working electrode. Like Iridium oxide film utilized in potentiometric measurement, the specific membrane is required to achieve a selection of targeted ions thus limiting the reaction. The auxiliary counter electrode provides the steady current path with no effect on the potential gap. The current induced which is a linear response to the concentration of the desired ions coming out of the working electrode can be measured by either a current conveyor circuit or an integrator converting current to a voltage signal for further processing.

Combining two separate circuits to achieve potentiometric and amperometric measurement within the same analyte solution environment is much more compact and efficient as the reference electrode is possible to be shared with potentiometric and amperometric potentiostat. As for potentiometric technique, sensed voltage at ion sensitive electrode is measured without a current pass. When the reference electrode is applied with stimulus voltage, resulting in induced current due to Faraday's law. Then the current and voltage relationship leads to polarization of the electrode that the potential across the electrode-electrolyte interface is dependent on the flowing current. To avoid this, the reference electrode is required to be non-polarizable interfacing with large current passing through meanwhile maintaining constant reaction area and stable concentration of the solution. Thus, the constant potential at the reference electrode is ensured.

Apart from specifying the characteristics of the reference electrode, the topology of potentiostat is also essential that the reference electrode is connected to the high impedance input terminal of the operational amplifier forming a positive feedback loop different from the configuration of potentiometric circuitry, which ensuring current flowing into working electrode rather than reference electrode. However, there are still some issues related to the shared reference configuration. The potential at the reference electrode can not reach the expected applied external voltage due to defects of the open-loop amplifying configuration. The potential difference existing between ion-sensitive electrode and reference electrode may be susceptible to other ions movement which forms amperometric current. It has been proved that those issues can be negligible regarding the continuous reading. Experiments carried out in [54] shows that potentiometric reading with shared reference electrode has extreme high correlation of 0.9981 with individual potentiometric measurement while correlation of combined and separate amperometric sensing results reach up to 0.9959, which indicate that the shared reference electrodes configuration is desirably feasible without being affected by the amperometric current flowing. The whole potentiostat topology is shown in Fig.3.2.

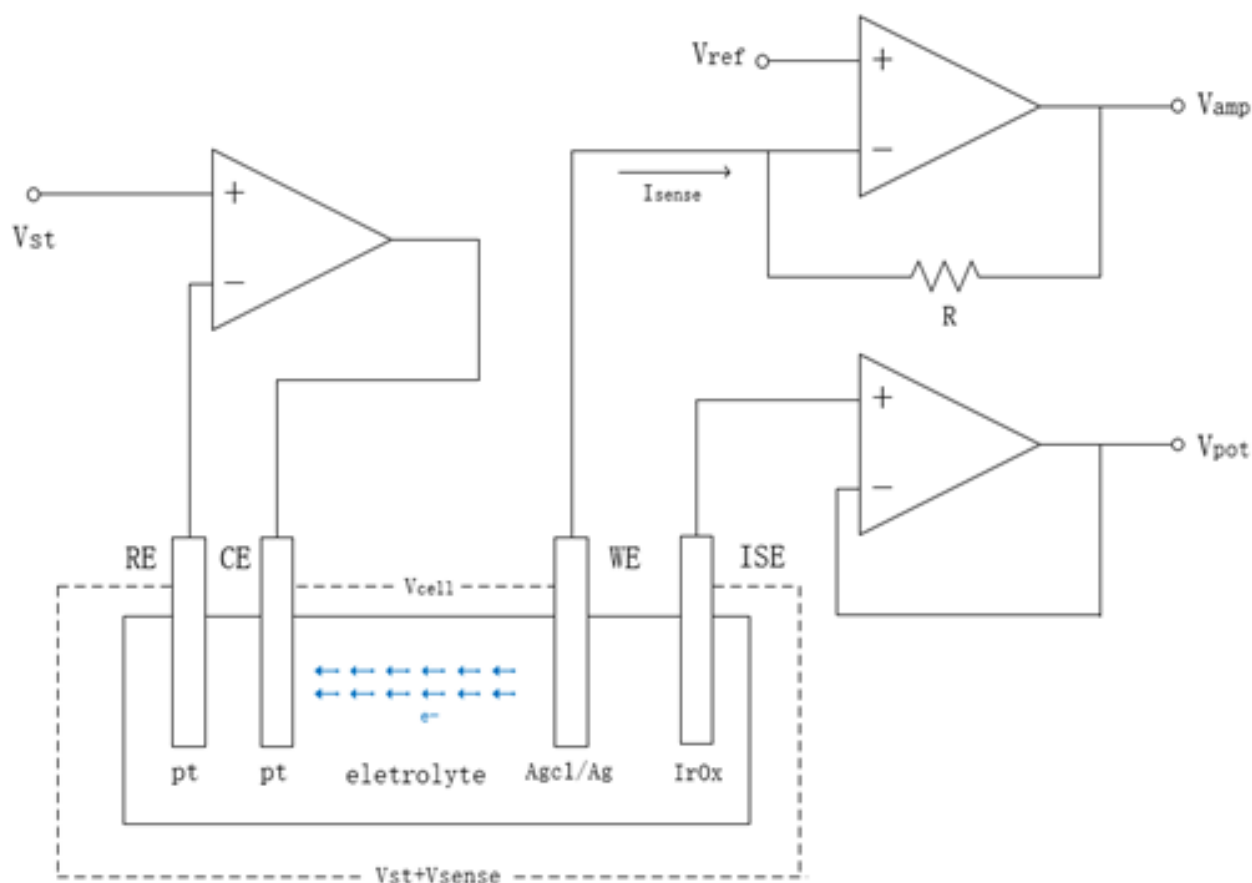


Figure 3.2: The structure of potentiostat with shared reference

### 3.3 Potentiometry

The potentiometric circuit composes of two blocks: voltage to current converter and currently starved ring oscillator shown in Fig.3.3. Potential at the ion-sensitive electrode is directly measured as the input voltage which contains the reference voltage plus the relative voltage induced from the biochemical reaction. After converting voltage into the current as the major impetus of oscillation, the current starved ring oscillator outputs the square wave signal with its frequency dependent on the driven current.

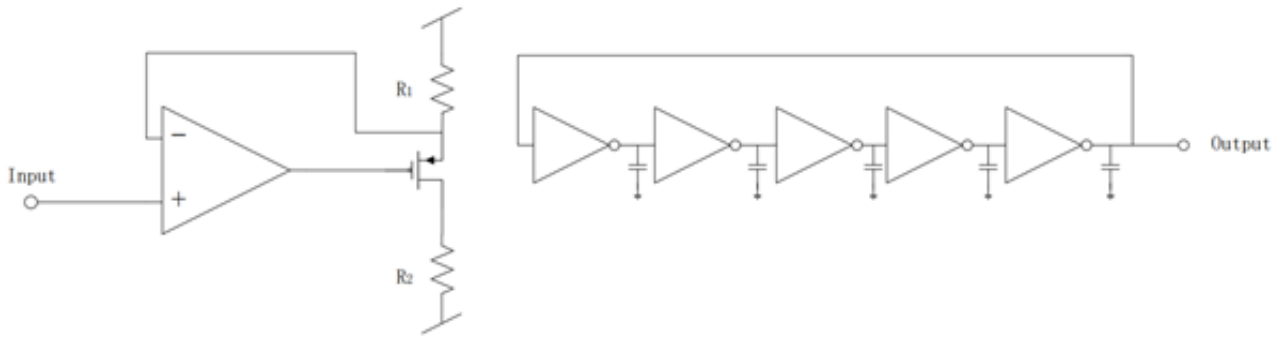


Figure 3.3: The structure of potentiometric circuitry

### 3.3.1 Voltage to current converter

Voltage to current converter relies on a similar current conveyor structure in which the input voltage is connected to the non-inverting terminal and output is directly linked to the gate of the pMOS transistor with its source feedback to the inverting terminal. According to the amplification formula:

$$V_G = A(V_{in} - V_S) \quad (3.1)$$

where,

$V_G$ : the gate voltage.

$A$ : the open-loop gain of the operational transconductance amplifier.

$V_{ref}$ : the input voltage.

$V_S$ : the source voltage.

Source voltage can be expressed as

$$V_S = V_{in} - \frac{V_G}{A} \quad (3.2)$$

where,

$V_G$ : the gate voltage.

$A$ : the open-loop gain of the operational transconductance amplifier.

$V_{ref}$ : the input voltage.

$V_S$ : the source voltage.

Also, source voltage conforms to the ohm's law:

$$V_S = V_{DD} - I_{ds}R_1 \quad (3.3)$$

where,

$R_1$ : the pull up resistance.

$V_{DD}$ : the power supply voltage.

$V_S$ : the source voltage.

Based on the relationship between current and gate to source voltage in saturated PMOS transistor regardless of second-order effect and body effect:

$$I_{ds} = \frac{1}{2}\beta(V_{GS} - V_{th})^2 \quad (3.4)$$

where,

$I_{ds}$ : the current through the channel.

$V_{GS}$ : the control voltage between gate and source.

$\beta$ : the constant related to the capacitance of oxide layer and aspect ratio of the transistor.

$V_{th}$ : the threshold voltage of PMOS.

Replacing the  $V_{GS}$  with the input voltage  $V_{in}$  and  $V_s$  with channel current  $I_{ds}$ :

$$I_{ds} = \frac{1}{2}\beta(AV_{in} - (A + 1)V_s - V_{th})^2 = \frac{1}{2}\beta(AV_{in} - (A + 1)(V_{DD} - I_{ds}R_1) - V_{th})^2 \quad (3.5)$$

where,

$I_{ds}$ : the current through the channel.

$V_{GS}$ : the control voltage between gate and source.

$\beta$ : the constant related to the capacitance of oxide layer and aspect ratio of the transistor.

$V_{th}$ : the threshold voltage of PMOS.

$R_1$ : the pull up resistance.

$A$ : the open-loop gain of the operational transconductance amplifier.

From intuitive observation on this formula, it is hard to obtain the relationship between channel current and input voltage. For simplicity, a certain approximation needs to be applied here. Back to the first formula, as the open-loop gain of the operational amplifier is ideally large that  $\frac{V_G}{A}$  can be neglected. Thus, the source voltage  $V_S$  approximately equals to the input voltage  $V_{in}$  ( $V_S = V_{in}$ ). Following equation 3.5 , the direct linear relationship can be obtained:

$$V_S = V_{DD} - I_{ds}R_1 = V_{in} \quad I_{ds} = -\frac{V_{IN}}{R_1} + \frac{V_{DD}}{R_1} \quad (3.6)$$

where,

$I_{ds}$ : the current through the channel.

$V_S$ : the source voltage.

$V_{DD}$ : the power supply voltage.

$R_1$ : the pull up resistance.

$V_{IN}$ : the input voltage.

The channel current is negatively proportional to input voltage with constant bias that linear conversion has been proved. As the resistor is better to be avoided using due to thermal noise source as well as large area, the resistor can be replaced by diode-connected MOSFET. In diode-connected MOSFET, the relationship is shown as:

$$\Delta V_{DS} = \Delta V_{GS} \Delta I_{DS} = gm \Delta V_{GS} \quad (3.7)$$

where,

$I_{DS}$ : the variation of voltage across channel.

$V_{DS}$ : the variation of current across channel.

$V_{GS}$ : the variation of voltage between gate and source.

$gm$ : the transconductance of MOSFET.

The equivalent resistance of diode-connected MOSFET:

$$R_{eq} = \frac{\Delta V_{DS}}{\Delta I_{DS}} = \frac{1}{gm} \quad (3.8)$$

where,

$R_{eq}$ : the equivalent resistance.

$I_{DS}$ : the variation of voltage across channel.

$V_{DS}$ : the variation of current across channel.

$V_{GS}$ : the variation of voltage between gate and source.

$gm$ : the transconductance of MOSFET.

The diode-connected MOSFET can be considered as a resistor of which equivalent resistance equals the reciprocal of the transconductance of MOSFET. The final linear relation between the input voltage and converted current is

$$I_{ds} = -gmV_{IN} + gmV_{DD} \quad (3.9)$$

where,

$I_{ds}$ : the current through the channel.

$V_{DD}$ : the power supply voltage.

$V_{IN}$ : the input voltage.

$gm$ : the transconductance of MOSFET.

As the transconductance is determined by the aspect ratio of the transistor and the current through the channel:

$$gm = \frac{\partial I_{ds}}{\partial V_{GS}} = \sqrt{2(\mu C_{ox})\left(\frac{W}{L}\right)I_D} \quad (3.10)$$

where,

$I_{ds}$ : the AC current through the channel.

$V_{GS}$ : the variation of voltage between gate and source.

$I_D$ : the DC current through the channel.

$C_{ox}$ : the capacitance of the oxide layer.

$\mu$ : the drift mobility of the carrier.

$W$  the width of the channel

$L$  : the length of the channel

$gm$ : the transconductance of MOSFET.

Therefore, the conversion ratio is positively proportional to  $\sqrt{\left(\frac{W}{L}\right)}$ . To achieve low power consumption, the aspect ratio  $\frac{W}{L}$  is set to be minimum that DC current through channel and variation of current is reduced.

### 3.3.2 Current starved ring oscillator

Traditional ring oscillator implements an odd number of inverters in series with the output of the last inverter fed back to the input of the first inverter. The oscillation period relies on the individual propagation delay of the inverter. To lower the oscillating frequency, there are two methods commonly used. First, making the ring from a larger number of inverters results in a lower frequency of oscillation, consuming the same power. Second, the external capacitors can be applied at the output of each stage along with the parasitic capacitor forming an integrated low pass filter with the channel resistance. The inverter can be expressed in an equivalent digital model shown in Fig.3.4 containing parasitic input capacitance, output capacitance, and channel resistance.

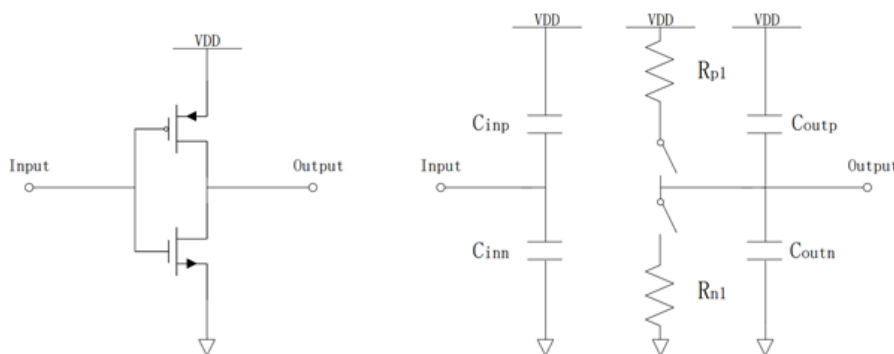


Figure 3.4: The equivalent digital model of inverter[7]

The effective input capacitance of the inverter is

$$C_{in} = \frac{3}{2}(C_{ox1} + C_{ox2}) = C_{inn} + C_{inp} \quad (3.11)$$

The effective output capacitance of the inverter is

$$C_{out} = C_{ox1} + C_{ox2} = C_{outn} + C_{outp} \quad (3.12)$$

When considering the charge and discharge process of individual inverter in ring oscillator, the capacitance on the inverters output or input is the sum of next inverter's input capacitance, last inverter's output capacitance and external capacitance

$$C_{tot} = C_{in} + C_{out} + C_{ext} = (C_{ox1} + C_{ox2}) + \frac{3}{2}(C_{ox1} + C_{ox2}) + C_{ext} = \frac{5}{2}(C_{ox1} + C_{ox2}) + C_{ext} \quad (3.13)$$

As the external capacitance is dominant which is much larger than parasitic total capacitance  $C_{ox1} + C_{ox2}$ , thus the total capacitance can be approximate to external capacitance.

$$C_{tot} \approx C_{ext} \quad (3.14)$$

The propagation delay of each inverter in ring oscillator is

$$t_p = t_{charge} + t_{discharge} = 0.7 \cdot R_n \cdot C_{ext} + 0.7 \cdot R_p \cdot C_{ext} = 0.7 \cdot (R_n + R_p) \cdot C_{ext} \quad (3.15)$$

where,

$t_p$ : the propagation delay of one inverter.

$R_n$ : the channel resistance of n type mosfet .

$R_p$ : the channel resistance of p type mosfet .

$C_{ext}$ : the added capacitance.

Based on a conventional ring oscillator, the current starved ring oscillator does not target to reduce total power consumption but also enables the frequency of output signal is linearly

proportional to the driven current to achieve linear conversion. The entire system is shown in Fig.3.5

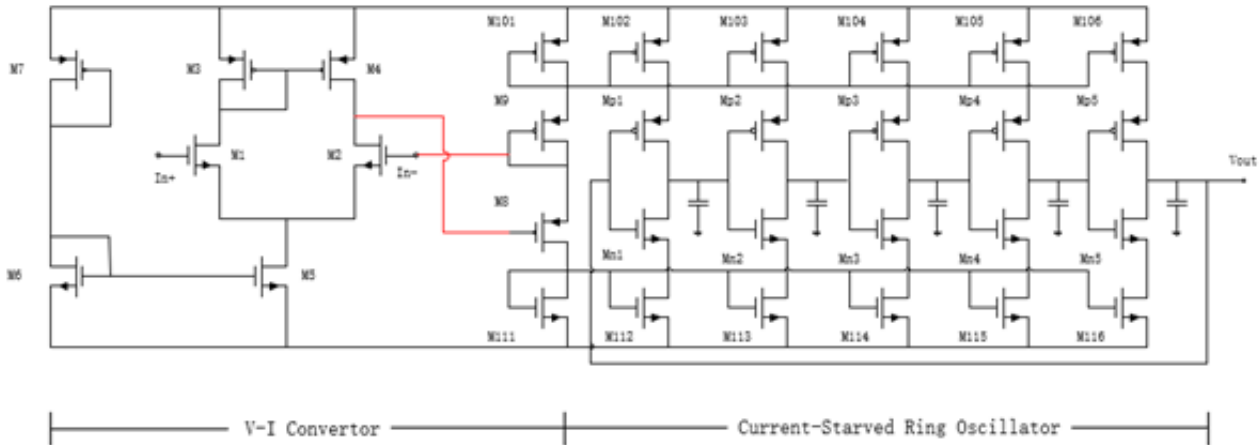


Figure 3.5: Schematic of potentiometric circuit

As is introduced before, the current is converted from input voltage through a quasi-current conveyor structure. To achieve current control of ring oscillator, current mirrors work as a current source and sink duplicating the converted current from the previous stage to charge and discharge the capacitor. Comparatively, power supply and channel resistance constitute a non-ideal current source in a traditional inverter, where the charging current is large and uncontrollable. The original inverter structure including pmos and nmos pairs work as a switch of which channel resistance is relatively low compared with the output resistance of the current source/sink shown in Fig.3.6. Thus, the aspect ratio  $\frac{W}{L}$  of the current source/sink is required to be much larger than that of switching MOSFET to allow lower consumption as well as enlarging output resistance

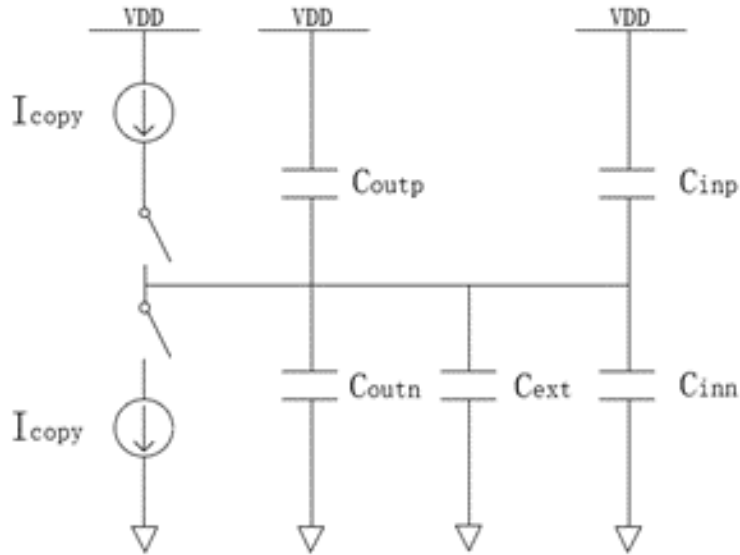


Figure 3.6: Digital model of inverter in current started ring oscillator

As is concluded before, the parasitic capacitance can be negligible relative to the external capacitance. Then the propagation delay of the individual inverter is

$$t_p = 2 \frac{V_{DD} C_{ext}}{I_{copy}} \quad (3.16)$$

where,

$t_p$ : the propagation delay of one inverter.

$I_{copy}$ : the converted current.

$V_{DD}$ : The power supply voltage.

$C_{ext}$ : the added capacitance.

The oscillation frequency then is given as

$$f_{osc} = \frac{1}{nt_p} = \frac{I_{copy}}{2nV_{DD}C_{ext}} = kI_{copy} \quad (3.17)$$

where,

$f_{osc}$ : the frequency of ring oscillator.

$n$ : the odd number of inverters connected in series.

$k$ : the constant

Thus, the linear relationship between converted current and output signal frequency has been proved. Combining equation.3.16 with equation.3.17:

$$f_{osc} = \frac{-gmV_{IN} + gmV_{DD} \left(\frac{W_2}{L_2}\right)}{2nV_{DD}C_{ext} \left(\frac{W_1}{L_1}\right)} \quad (3.18)$$

where,

$f_{osc}$ : the frequency of ring oscillator.

$V_{DD}$ : The power supply voltage.

$V_{IN}$ : The input voltage.

$n$ : the odd number of inverters connected in series.

$gm$ : the transconductance of MOSFET.

$C_{ext}$ : the extra capacitance.

The potentiometric measurement has been demonstrated the linear conversion from input sensing voltage to output signal frequency.

### 3.4 Amperometry

The amperometric circuit implements a first-order incremental sigma-delta ( $\Sigma\Delta$ ) ADC structure with two major components consisting: switched capacitor integrator and comparator, which generates a high-speed square wave with its frequency linearly responding to the input sensing current. The output of the comparator is fed back to control the switch parallel with the capacitor enabling resetting of the capacitor and forcing the integrator to drop the ramp output down, forming a triangular oscillating waveform ranged between the reference voltage of the integrator and the reference of the comparator.

Similar to conventional sigma-delta ( $\Sigma\Delta$ ) ADC, there are two phases of the entire system including integration and reset. Additional power-on pulse is provided externally through an or gate with another input connected with comparator output, to start up the system initially at

integration mode. When the comparator outputs high, the switch is closed leaving a configured voltage buffer. With the negative feedback, the output of the integrator is forced to be the same as reference voltage  $int_{ref}$  at the non-inverting terminal of the integrator rising at constant speed until the output of the comparator toggles. Then the switch is open leaving a simple integrator configuration. Sensing current will be integrated through the capacitor. Since the potential at the left plate of the capacitor connected to the electrode is fixed, accumulation on the capacitor makes output drop to form potential difference till the output reaches the reference voltage  $comp_{ref}$  at inverting terminal of the comparator. The comparator toggles again closing the switch and re-entering the reset mode.

The resulted oscillating waveform is shown in Fig.3.7

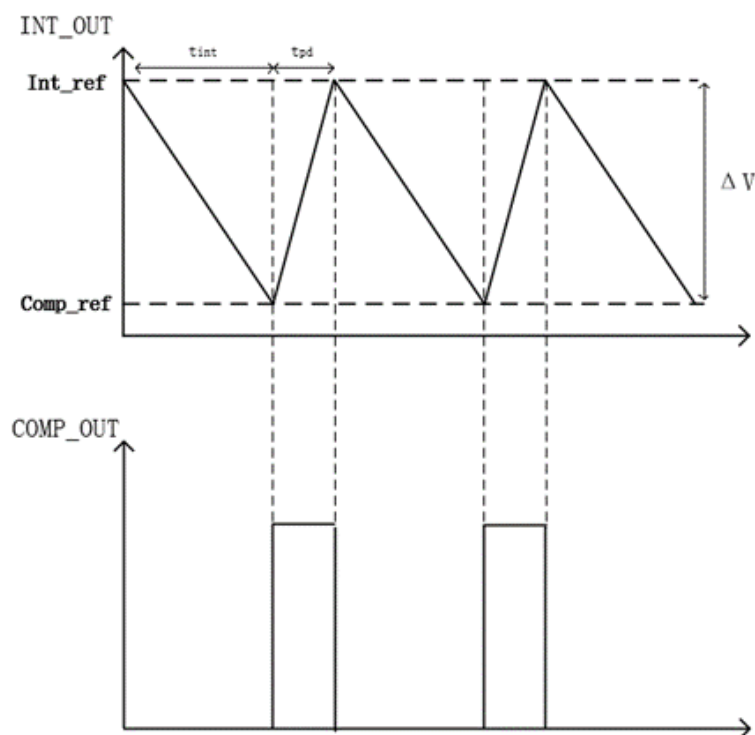


Figure 3.7: Waveform of amperometric output

The period of the oscillating wave is composed of two-time phases:  $t_{int}$  and  $t_{pd}$ .  $t_{int}$  represents the period of integration phase and  $t_{pd}$  represents the period of propagation delay time or reset phase. Integration time depends on the magnitude of sensing current as well as

the capacitance of integrator capacitor, expressed by the equation:

$$t_{int} = \frac{C\Delta V}{I_{sense}} \quad (3.19)$$

where,

$t_{int}$ : the integration time over one period.

$I_{sense}$ : sensing current from electrode.

$\Delta V$ : The potential variation.

The total period of the oscillation is

$$t_{osc} = t_{int} + t_{pd} \quad (3.20)$$

where,

$t_{int}$ : the integration time over one period.

$t_{pd}$ : the propagation delay of comparator.

As the propagation delay  $t_{pd}$  is far smaller than  $t_{int}$  which can be considered negligible that

$$t_{osc} \approx t_{int} \quad (3.21)$$

The frequency of the output signal then is expressed as

$$f_{osc} = \frac{1}{t_{int}} = \frac{I_{sense}}{C(V_{int-ref} - V_{com-ref})} \quad (3.22)$$

Which is linear proportional to the magnitude of sensing current and can be adjusted by changing the capacitance and difference between reference voltages. However, the propagation delay influences the linearity of the translation curve that when integration time tends to be small.

### 3.5 Mixing signal

To mix up the amperometric and potentiometric signals, normally a simple NAND gate can be used. However, the duty cycle of amperometric signal is not 50% that is not easy for demodulation at the backend. Therefore d-type flip flop configured as 1-bit counter outputs 50% duty cycle signal where potentiometric signal is connected to the reset port of DFF while amperometric signal is set as a driven clock signal. Since the DFF flipping over is triggered by the rising edge of the clock signal, the 50% output signal can be achieved regardless of the duty cycle of the clock signal.

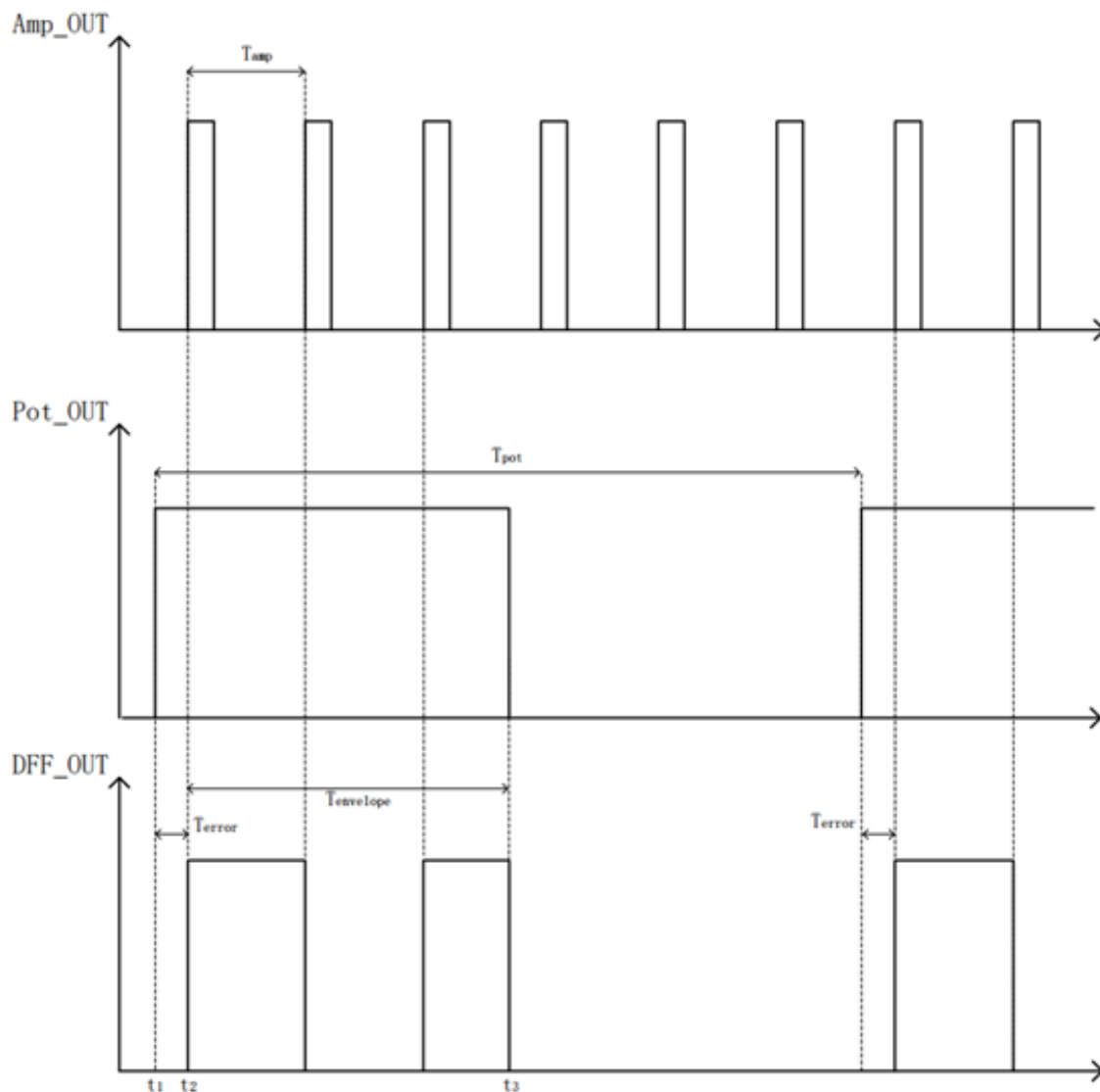


Figure 3.8: Waveform of mixed signal

Ideally, the amperometric and potentiometric signals are in a phase that the envelope of the output signal reflects the accurate frequency of the potentiometric signal. However, there is a phase difference between two input signals, hence causing certain errors. Supposing the potentiometric signal rises just after the amperometric reaches the high level, DFF misses the opportunity to record the first clock in until the next clock rising edge shown in Fig.3.8. The maximum error is one period of the amperometric signal which is unavoidable. The envelope of received signal related to error can be expressed as

$$T_{envelop} = t_3 - t_2 = (t_3 - t_1) - (t_2 - t_1) = \frac{T_{pot}}{2} - T_{error} \quad (3.23)$$

$$T_{envelop} \in \left[ \frac{T_{pot}}{2} - T_{amp}, \frac{T_{pot}}{2} \right] \quad (3.24)$$

To minimize the influence of the error and approach envelope of output signal close to half of the potentiometric signal, the frequency gap needs to be extended as large as possible. By making the amperometric frequency 20 times larger than the potentiometric frequency, the percentage error can be reduced to 5%, which is more accurate and acceptable. As the period of amperometric signal is also related to the propagation delay, to achieve better accuracy, the propagation delay is required to be as small as possible, resulting in enlarging the comparator's slew rate and amplifying gain.

# Chapter 4

## Improved potentiometric and amperometric readout circuits system

### 4.1 Adapted voltage to current converter

#### 4.1.1 Structures

THE V-to-I converter implements the current conveyor structure as mentioned before with current mirrors copying the converted current and outputting to the current-controlled oscillator shown in Fig.4.1.

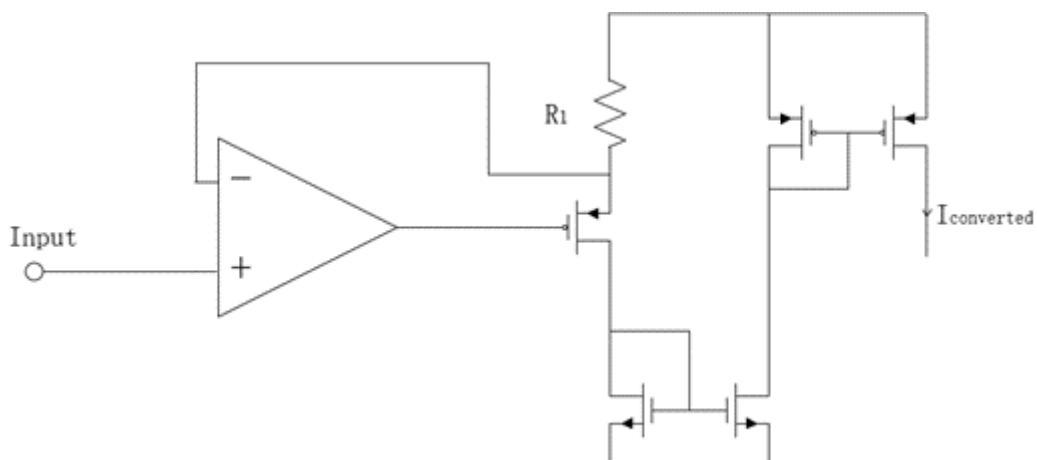


Figure 4.1: Structure of voltage-to-current converter

The schematic is shown in Fig.4.2 with several modifications:

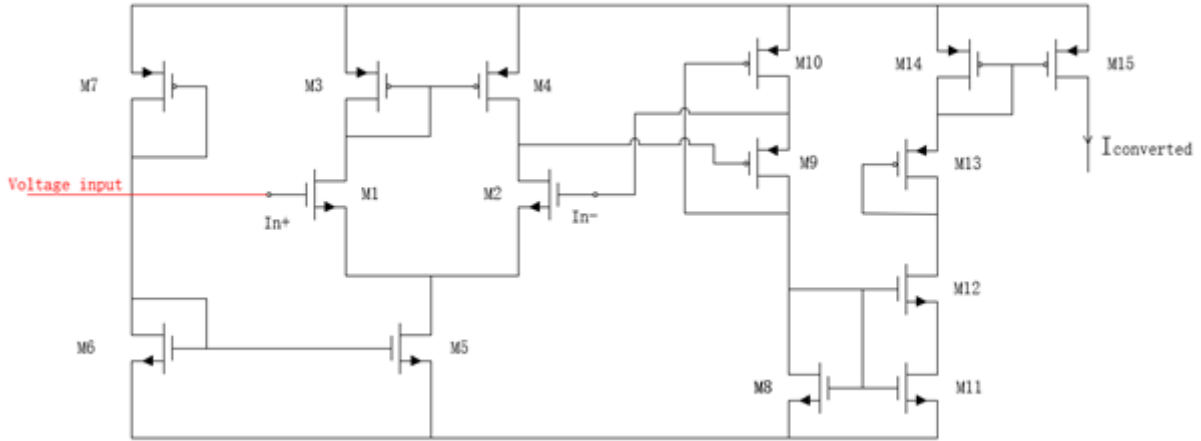


Figure 4.2: Schematic of adapted voltage-to-current converter

### 4.1.2 Principles

The single-stage differential pair is biased with current through diode-connected transistor M7 which functions as a linear resistor. To achieve the lowest power consumption, the length of M7 stretches to 20um and the width of M7 is reduced to a minimum 220nm within a valid range to have max equivalent resistance. Similarly, the ratio of M10 is also set to be 220nm/20um and the gate of transistor M10 is connected to the drain of M9, making the M10 work in the deep triode region achieving larger equivalent resistance. The current through transistor working in triode region can be expressed as:

$$i_D = \mu_p C_{OX} \frac{W}{L} [(V_{GS} - V_{th}) V_{DS} - \frac{1}{2} V_{DS}^2] \quad (4.1)$$

where,

$I_D$ : the AC current through the channel.

$V_{GS}$ : the control voltage between gate and source.

$V_{DS}$ : the potential difference between drain and source.

$V_{th}$ : the threshold voltage of transistor.

$C_{ox}$ : the capacitance of the oxide layer.

$\mu_p$ : the drift mobility of the holes.

$W$  the width of the channel

$L$  : the length of the channel

When  $V_{DS}$  is relatively small that  $V_{DS} \ll V_{GS} - V_{th}$  when gate of M10 is connected to the drain of M9, the current  $i_D$  then can be expressed as

$$i_D = \mu_p C_{OX} \frac{W}{L} [(V_{GS} - V_{th}) V_{DS}] \quad (4.2)$$

The channel resistance  $r_D$  can be denoted as

$$r_D = \frac{V_{DS}}{i_D} = \frac{1}{\mu_p C_{OX} \frac{W}{L} (V_{GS} - V_{th})} \quad (4.3)$$

The override voltage  $V_{GS} - V_{th}$  is treated as a constant with a small current variation. The source voltage of M9 is fixed at input voltage due to negative feedback from the differential pair amplifier. Then the current through M9 can be denoted through ohm's law:

$$I_D = \frac{V_{DD} - V_S}{r_D} = \frac{V_{DD} - V_{input}}{r_D} = (V_{DD} - V_{input}) \mu_p C_{OX} \frac{W_{10}}{L_{10}} (V_{GS} - V_{th}) \quad (4.4)$$

where,

$I_D$ : the current through the channel.

$r_D$ : the channel resistance.

$V_{GS}$ : the control voltage between gate and source.

$V_{input}$ : the input voltage.

$V_{th}$ : the threshold voltage of transistor.

$C_{ox}$ : the capacitance of the oxide layer.

$\mu_p$ : the drift mobility of the holes.

$W_{10}$  the width of transistor M10

$L_{10}$  : the length of transistor M10

M8, M11, and M12 constitute current mirror amplifies the current with less than 1 gain based on the ratio between their aspect ratios. M11 connected M12 works as an integrated transistor with a combined channel length. M13 is diode-connected working as a resistor which does not affect the magnitude of current pass through. The transistor M14 has an identical size with M15 to ensure 1:1 duplication of the current. The relationship between the current through M8 and converted current is shown in the equation:

$$\frac{I_D}{I_{converted}} = \frac{W_8}{L_8} \frac{W_{11}}{(L_{11} + L_{12})} \quad (4.5)$$

where,

$I_D$ : the current through the transistor M8.

$I_D$ : the current through the transistor M11.

$W_8$  the width of transistor M8

$L_8$  : the length of transistor M8

$W_{11}$  the width of transistor M11

$L_{11}$  : the length of transistor M11

$L_{12}$  : the length of transistor M12

The relation of converted current and input voltage can be expressed as:

$$I_{converted} = \frac{W_{11}W_{10}L_8}{W_8L_{10}(L_{11} + L_{12})} \mu_p C_{OX} (V_{GS} - V_{th})(V_{DD} - V_{input}) = KV_{input} + B \quad (4.6)$$

$$K = -\frac{W_{11}W_{10}L_8}{W_8L_{10}(L_{11} + L_{12})} \mu_p C_{OX} (V_{GS} - V_{th}) \quad (4.7)$$

$$B = \frac{W_{11}W_{10}L_8}{W_8L_{10}(L_{11} + L_{12})} \mu_p C_{OX} (V_{GS} - V_{th})V_{DD} \quad (4.8)$$

Where,

K and B are numerical constant.

Therefore, the linear conversion from voltage to current has been demonstrated. Compared with the previously adopted voltage to current converter, the total current is further reduced hence resulting in lower power dissipation. The nonlinearity comes from the imperfect amplification gain of differential pair amplifier that the source of M9 is not the same as input voltage. As one of the key determinations on amplification gain of differential pair is the bias current which is also required to be as small as possible to boost power efficiency, there is a trade-off between linearity and power consumption. Apart from that, non-linearity is also caused by the unfixed potential  $V_{GS}$  between gate and source of M10. The gate voltage of M10 is the same as the drain voltage of M9 and the drain voltage of M8. When the current varies, the drain voltage of M8 also fluctuates. If the current is very small, the drain voltage of M8 can be considered as constant. When it comes to large currents, the variation of drain voltage cannot be neglected. Thus, when the input voltage is very small the converted current is very large, the linearity around this point is poor.

### 4.1.3 Simulation results

The voltage to current converter is designed in TSMC180BCD technology with supply voltage at 1.4V. According to the schematics shown in Fig.4.6, the sizes of M1 and M2 of the differential pair are set to be 60um/180nm, and the active load M3,M4 are set to be 4um/360nm. The current mirror M5,M6 supplying biasing current are set to 5um/1um and 10um/1um to achieve halving the current. M7,M9,M10 working as a linear resistor are set to 220nm/20um in diode-connection. M8 and M11,M12 consist current mirror reduce current with large gain which are set to 88um/1um and 220nm/20um respectively. All the sizes of transistors are listed in the table

Table 4.1: Sizes of transistors in the voltage-to-current converter circuits

MOSFETs	W/L
M1,M2	60um/180nm
M3,M4	4um/360nm
M5	5um/1um
M6	10um/1um
M8	88um/1um
M7,M9,M10,M11,M12	220nm/20um
M13	2um/10um
M14	4um/1um

The simulated results are shown in the Fig.4.3 compared with the ideal converted current curve versus input voltage

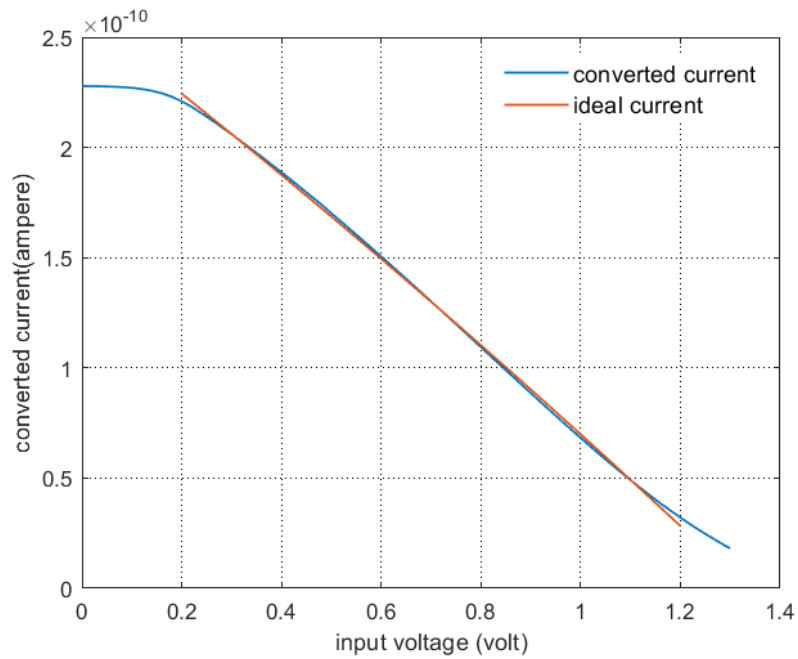


Figure 4.3: Converted current vs input voltage

The plot has shown very high linearity within range between 0.2V and 1.2V with the high correlation of 0.9994.

## 4.2 Improved current controlled oscillator in amperometry

The current starved ring oscillator used in original potentiometric measurement implements the summation of the propagation delay of each inverter where 5 inverters are used with large capacitors (10pF) at the output of each inverter and current source and sink for each inverter, resulting in taking up a large area. It is redundant to have each inverter equipped with a current source and sink which increases power consumption.

To boost the power efficiency, an improved current-controlled oscillator is introduced consisting of 8 inverters in total to realize linear current to frequency conversion. The structure is illustrated as Fig.4.4:

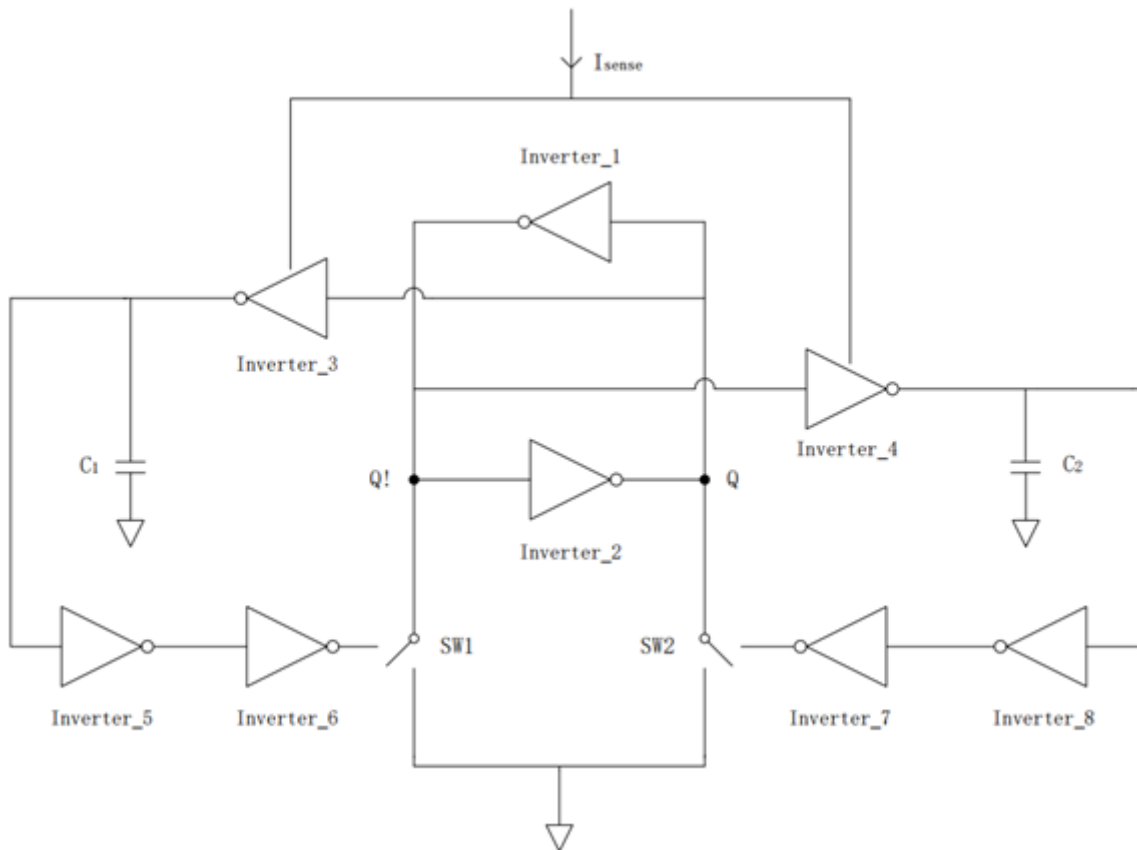


Figure 4.4: Structure of improved current controlled oscillator

The inverters are named from Inverter\_1 to Inverter\_8; The inverter\_3 and inverter\_4

connected with capacitor C1 and C2 respectively are key to the oscillation where the capacitors charge with injection current and discharge instantly controlled by the SRAM structured inverter pairs. The charging and discharging process are depicted as Fig.4.5:

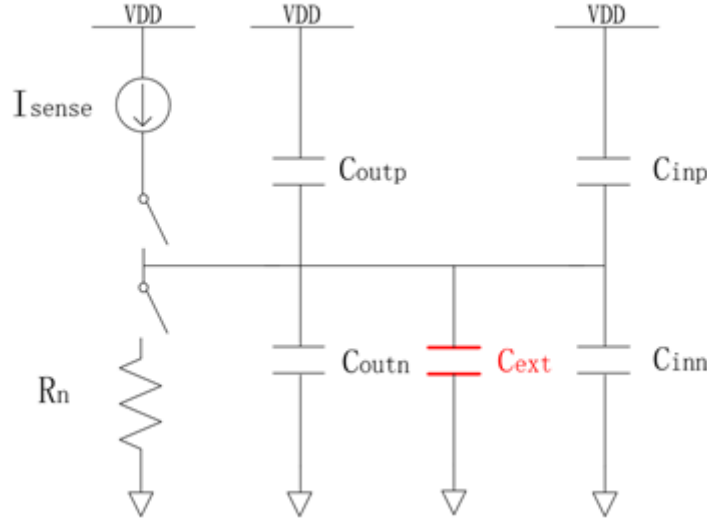


Figure 4.5: Digital model of inverter in improved current controlled oscillator

When the upper switch is closed while the downer switch is open, the sensed current starts to charge the parasitic and external capacitors. The charging time can be expressed as

$$t_{charge} = \frac{\Delta V(C_{ext} + C_{para})}{I_{sense}} \quad (4.9)$$

where,

$t_{charge}$ : the charging time of inverter.

$I_{sense}$ : the injected sensing current from the electrode.

$\Delta V$ : the maximum voltage of the capacitor which can be reached during charging.

$C_{ext}$ : the added external capacitance.

$C_{para}$ : the parasitic capacitance including output capacitance of the inverter and output capacitance of the next stage.

As the capacitance of the added capacitor is much larger than parasitic capacitance. The  $C_{para}$  can be ignored in the charging time calculation. Thus, the charging time can be expressed

as:

$$t_{charge} = \frac{C_{ext}\Delta V}{I_{sense}} \quad (4.10)$$

The maximum voltage the capacitor can reach is determined by the switching point of the next stage which is ideally half power supply 0.7V but varies depending on the magnitude of injected current following experimental results, which is discussed later.

When the upper switch is open and the downer switch is closed. The external capacitor which is dominant starts to discharge through channel resistance of nmos with the discharging time constant  $\tau$  expressed as

$$\tau = C_{ext}R_n \quad (4.11)$$

According to the measurement, time constant time is very small compared with charging time, the discharging process is considered instantaneous. Inverter\_5 in series with inverter\_6 and inverter\_7 in series with inverter\_8 work as voltage buffer while introducing propagation delay to turn on and off the switches. Inverter\_1 and inverter\_2 constitute a basic one-bit SRAM cell in a cross-coupled connection. There are two stable states 0 and 1 with the access transistor controlled by the signal buffered from the ramping up potential on the capacitor.

By observing the schematic of the entire oscillator shown in Fig.4.6, the SRAM cell is a key component to store and output 1 and 0 periodically.

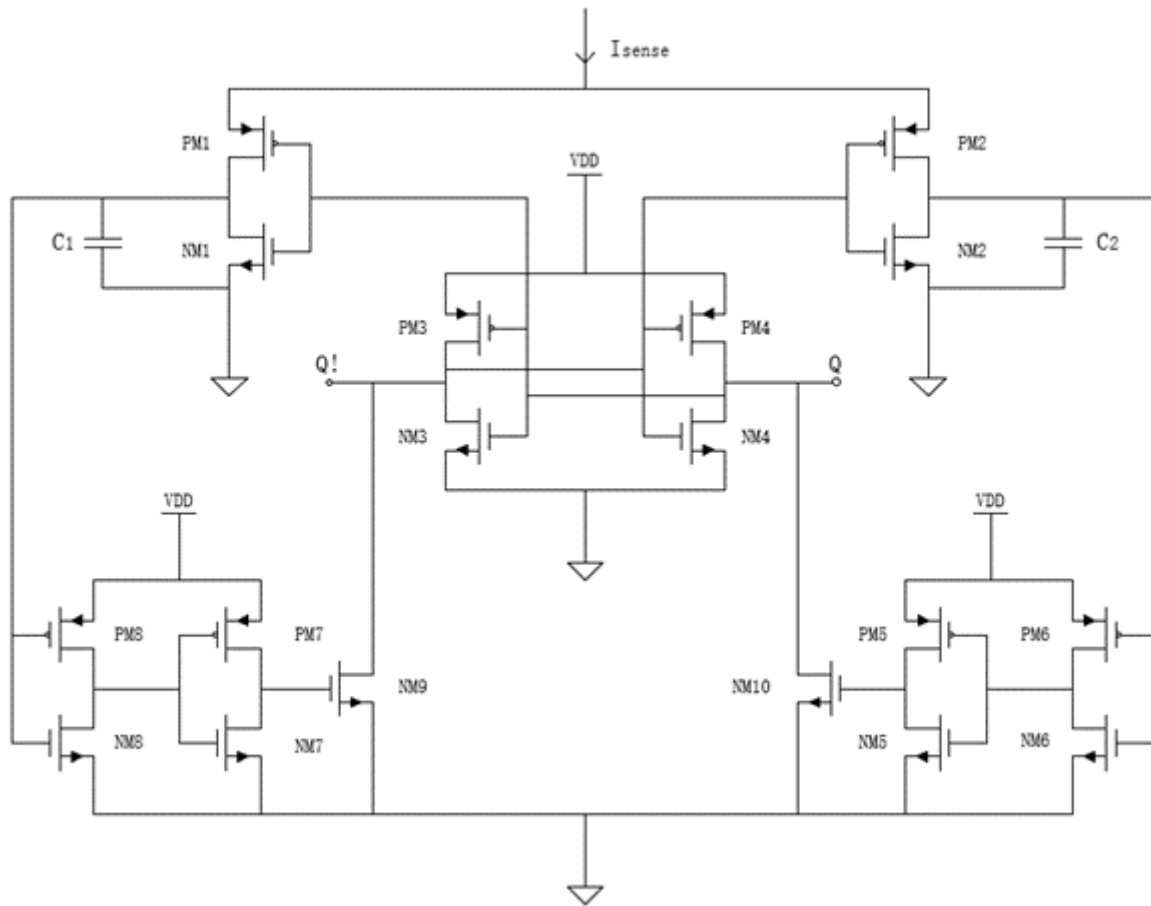


Figure 4.6: Schematic of improved current controlled oscillator

When the SW1 which is a nmos NM9 in the schematic is closed, the Q! state is pulled down to a low level forcing Q output high level. The high-level signal Q switches off the MOSFET PM1 and switches on the NM1 allowing the capacitor C1 discharge while low-level Q! switches on the PM2 and off the NM2, charging capacitor C2. As the discharging is instantaneous, the control signal on NM9 buffered from potential C1 suddenly drops to zero, switching the NM9 off. The SRAM bit cell finishes the writing mode and entering the store mode with terminal Q outputting 1 and terminal Q! outputting 0 during this period. The capacitor C2 charges up at a steady speed with injected DC sensing current until reaching the switching point of the buffer. Then NM10 is incompletely turned on under control signal just over switching point, writing 0 to SRAM bit cell where Q output 0 and Q! output 1. The repetition of the whole process takes the duration of the charging time to flip over the output and utilize the SRAM bit cell to maintain the output over this period. The resulted output of the oscillator is a square

wave with 50% duty cycle if the sizes of capacitors are the same. The waveform at each point including potential at capacitor C1, potential at capacitor C, output of terminal Q, and output of terminal Q! can be visualized in Fig.4.7 :

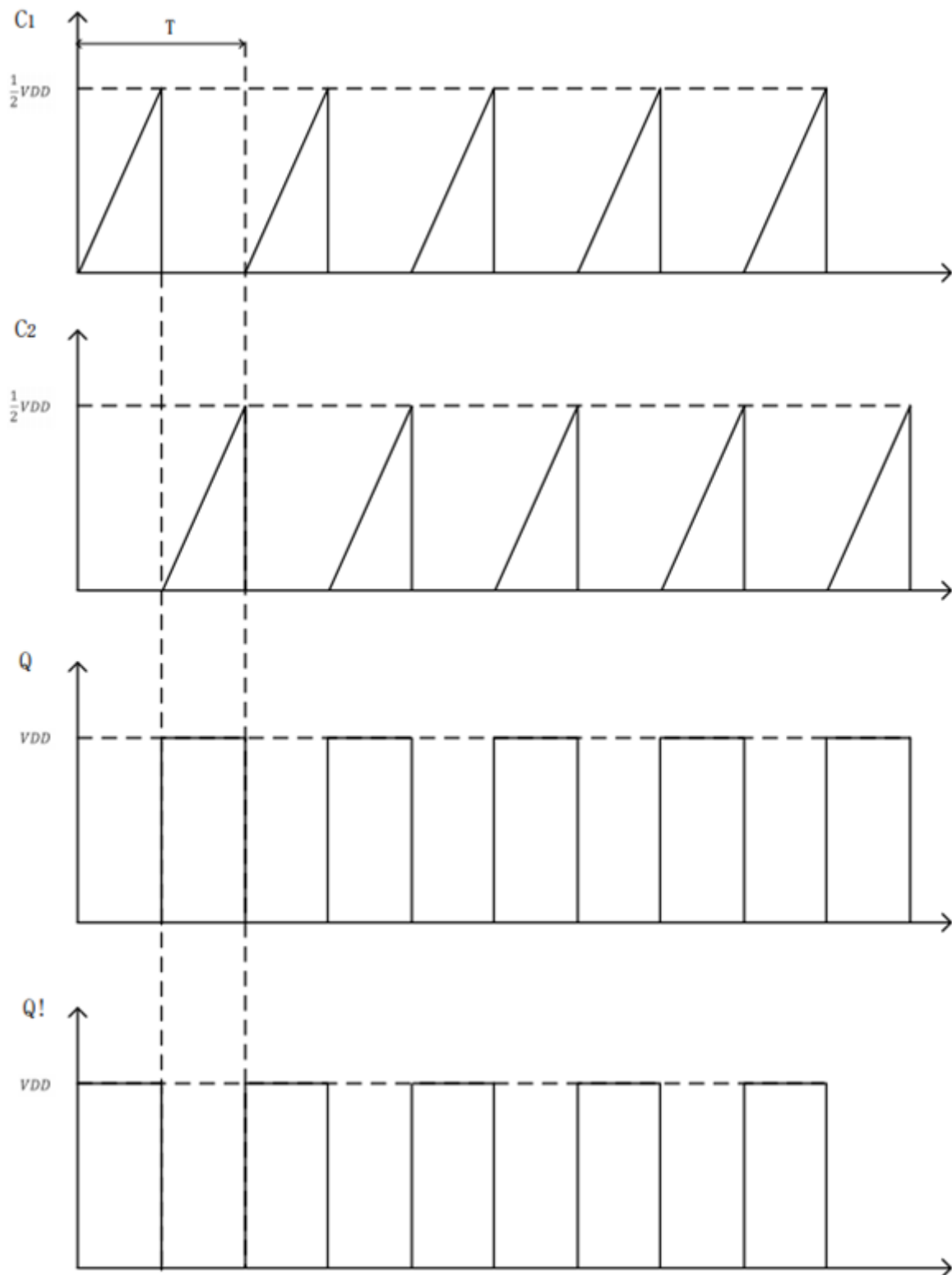


Figure 4.7: Output waveform of improved current controlled oscillator

Period of oscillation equals to twice charging time which is expressed in equation:

$$T = 2t_{charge} = \frac{2C_{ext}\Delta V}{I_{sense}} = \frac{C_{ext}V_{DD}}{I_{sense}} \quad (4.12)$$

where,

$t_{charge}$ : the charging time of inverter.

$I_{sense}$ : the injected sensing current from the electrode.

$\Delta V$ : the maximum voltage of the capacitor which can be reached during charging.

$V_{DD}$ : the power supply voltage.

$C_{ext}$ : the added external capacitance.

Then the frequency of oscillation is denoted as

$$f_{osc} = \frac{I_{sense}}{C_{ext}V_{DD}} \quad (4.13)$$

Therefore, the linear conversion from current to frequency has been approved with simple modifiable parameters: the external capacitance and the power supply voltage.

To further increase the oscillation frequency with a given sensing current, external capacitance needs to be reduced. However, the capacitance cannot be too small to avoid the influence of parasitic capacitance. The desirable applied power supply voltage  $V_{DD}$  is 1.4V related to the threshold voltage of NMOS and PMOS in the given foundry. The validity of this equation relies on the fact that the switching point of the buffer is 0.7V which is the half-power supply voltage and large enough to turn the switch on. When it comes to high frequency, the propagation delay of the buffer will start to be non-negligible that the obtained output signal frequency is smaller than the speculated, which is the source of non-linearity of the current to frequency conversion

This current-to-frequency converter can be used in amperometry with the capability of handling a large dynamic range of current input with the output frequency tuned by the

external capacitance. Connected with a voltage to the current convertor, this converter can be also applied in potentiometry.

### 4.2.1 Simulation results

The whole circuits are completely symmetric in that the half side of the transistors have identical ratio sizes with the other half side. Inverter\_1 consisting of PM1 and NM1(PM2 and NM2) works as a switch to change the charge and discharge direction, of which size are set to be small: 800nm/180nm and 400nm/180nm. (PM3,NM3) and (PM4,NM4) are used to store data bit which are set to be larger for fast switching requirements. NM9 and NM10 function as a switch to discharge the output equivalent to writing 0 bit to SRAM cell, which is set to be small size 2.18um/180nm as well. The sizes of the rest transistors are listed in the table below.

Table 4.2: Sizes of transistors in the current controlled oscillator

<b>MOSFETs</b>	<b>W/L</b>
PM1,PM2	800nm/180nm
NM1,NM2	400nm/180nm
PM3,PM4	4um/1um
NM3,NM4	2um/1um
PM5,PM6,PM7,PM8	10um/3.4um
NM5,NM6,NM7,NM8	2.5um/3.4um
NM9,NM10	2.18um/180nm

The obtained frequency with input current ranging from 100pA to 10μA are shown in the Fig.4.8 and the power consumption versus input current shown in the Fig.4.9.

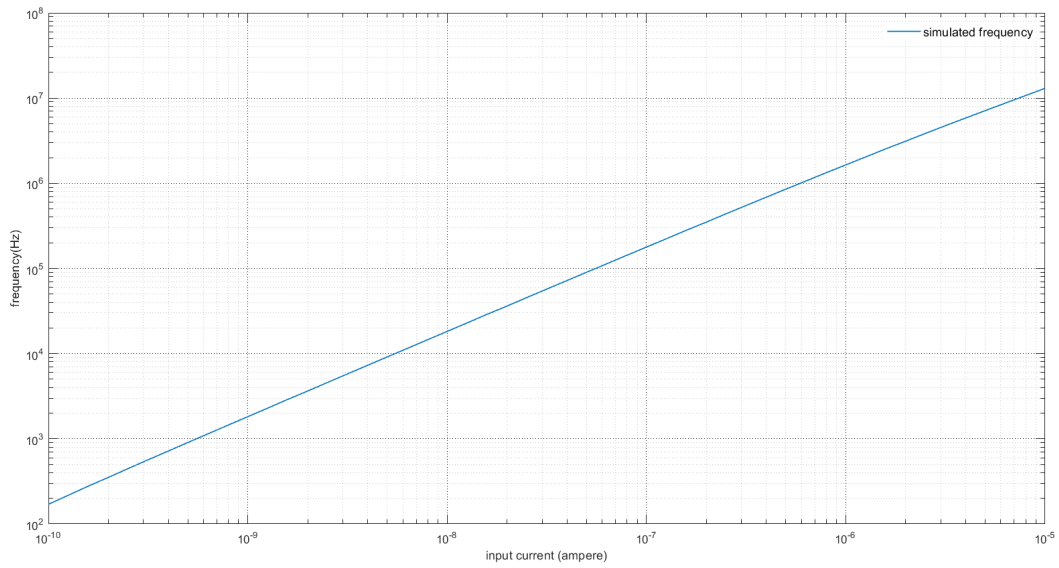


Figure 4.8: Systematic simulation results for current-to-frequency

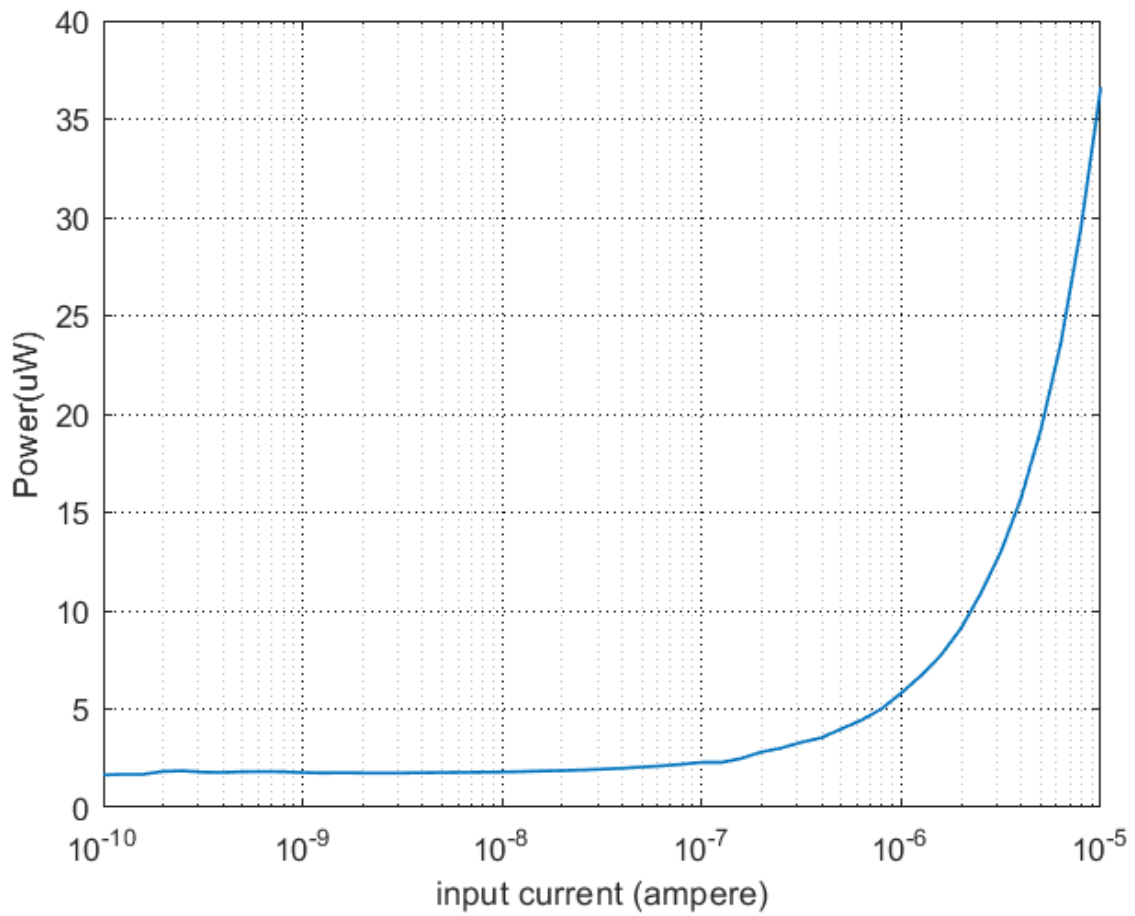


Figure 4.9: Power consumption in current-to-frequency converter

The linearity of current to frequency is desirable while the power consumption starts to increase sharply when input current reaches microampere( $\mu A$ ) level. To balance the power consumption and input linear range, the upper limit input current is set to be  $1\mu A$ , where the power consumption is around  $5\mu W$ . The comparison between ideal conversion curve and simulated curve is shown in Fig.4.10

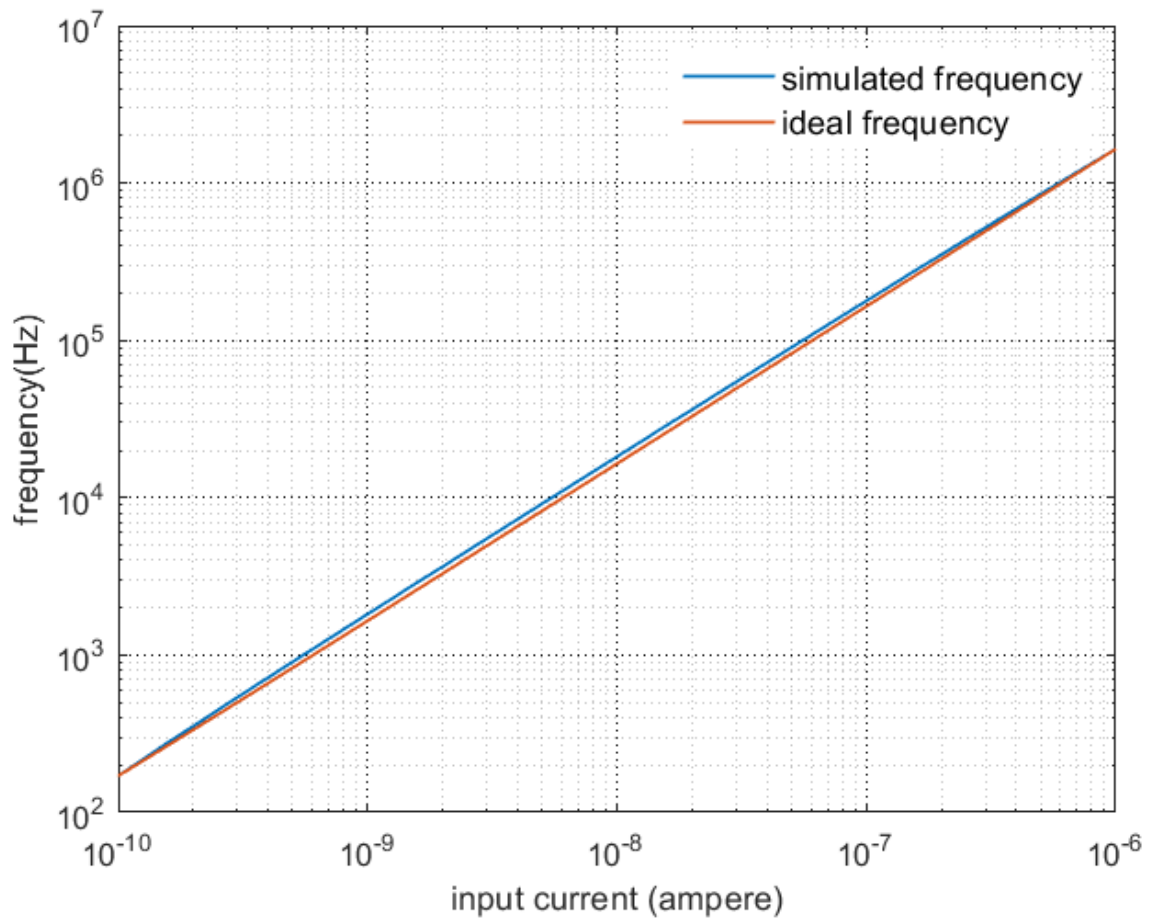


Figure 4.10: Ideal curve versus simulated curve

The correlation between them is measure as 0.9990 which proves the high linearity of current to frequency conversion. The maximum power consumption is  $5.81\mu W$ .



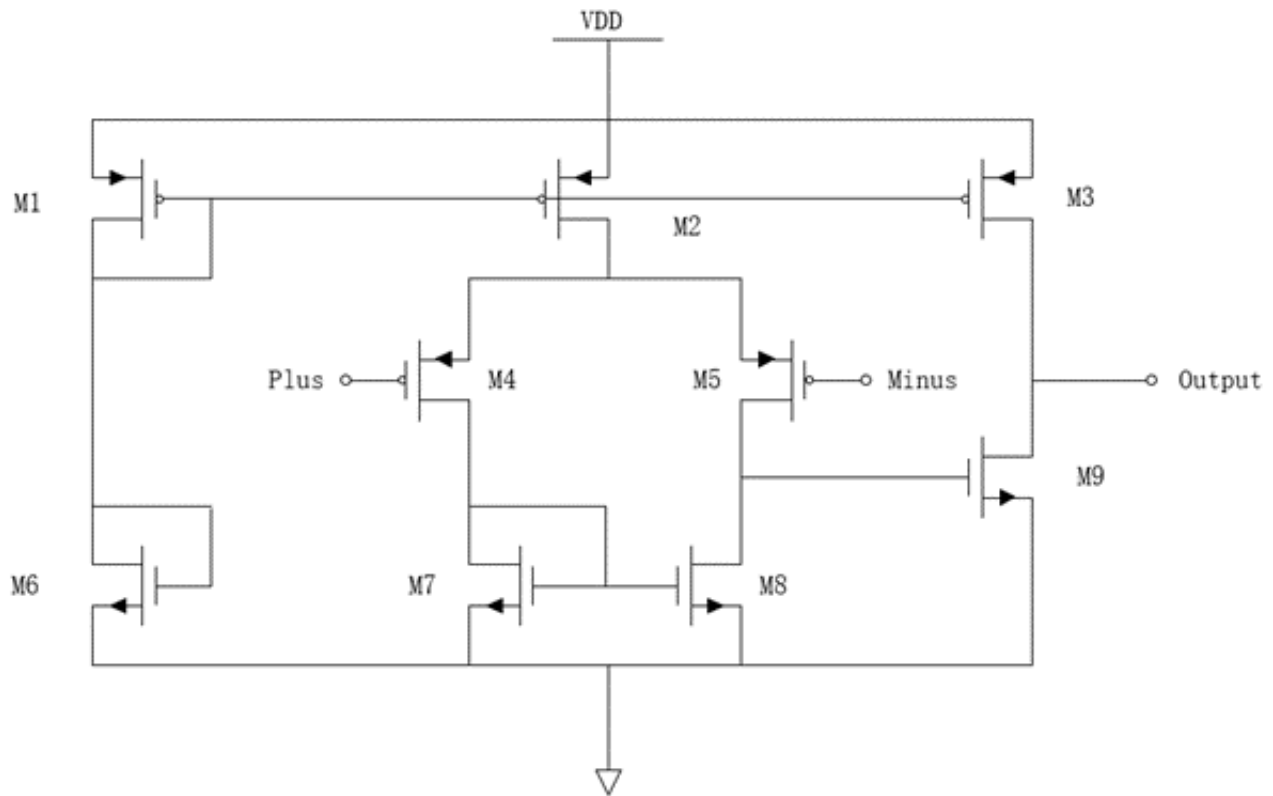


Figure 4.12: Schematic of PMOS comparator

### 4.3.2 Principles

Having a similar principle with the previous current controlled oscillator, this circuitry also implements the feedback to charge and discharge the capacitor. The two inverters linked in series on the right output two opposite phase clock signals CLK and CLK! respectively regarded as an output signal. Supposing the CLK signal is high and CLK! signal is low, the transistor PM2 is turned on and transistor PM1 is turned off, where PM2 is only one current path for input current to flow through. PM3 and NM1 are turned on simultaneously, leaving the non-inverting terminal of the comparator connected to the capacitor and inverting terminal of the comparator connected to the reference voltage supplied externally. As the potential at capacitor C1 is zero at this moment which is far less than the reference voltage, the comparator outputs low-level signal that the CLK still maintains a high level after inverting. Meanwhile, the NM4 is turned on, making capacitor C2 short-circuited leading to a sudden drop of potential. When the potential of the capacitor keeps increasing until exceeding the reference voltage, the comparator

toggles to flip over the states of CLK and CLK!. The current path PM2 is then shut down and PM1 and PM4 alternatively turned on, providing another current path to charge capacitor C2 up. The reference voltage switches to the non-inverting terminal while the inverting terminal is connected to capacitor C2 at which the potential is zero. The comparator outputs a high level without change until the potential of capacitor C2 catches up with the reference voltage. After repetition of two working modes, the oscillation is then generated with the reference shown in Fig.4.13 which is very similar to the output of the previous current controlled oscillator but with varied potential, the capacitor can reach.

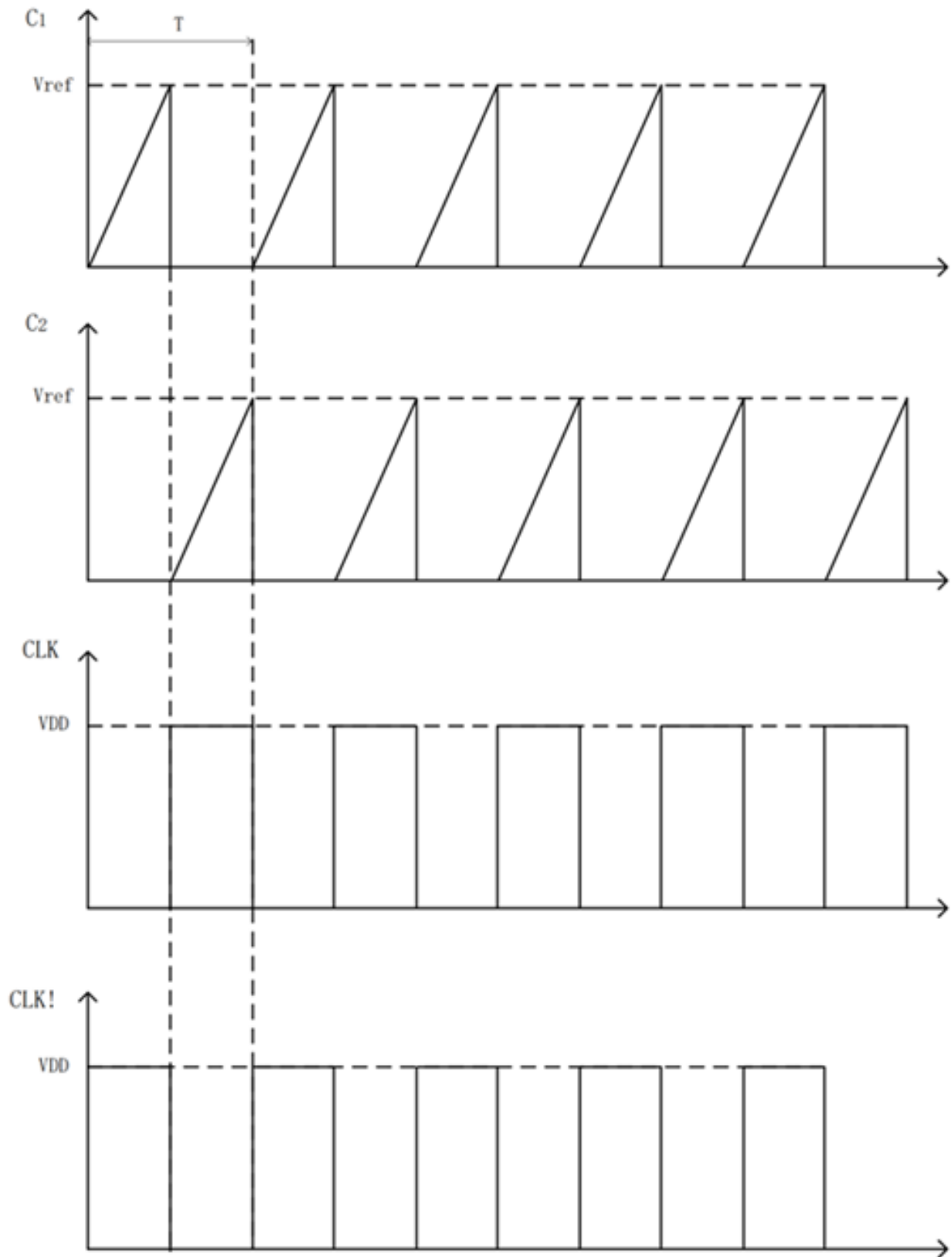


Figure 4.13: Waveform of renewed current controlled oscillator

Period of oscillation equals twice charging time which is expressed in equation:

$$T = 2t_{charge} = \frac{2C_{ext}\Delta V}{I_{input}} = \frac{2C_{ext}V_{ref}}{I_{input}} \quad (4.14)$$

where,

$t_{charge}$ : the charging time of inverter.

$I_{sense}$ : the injected sensing current from the electrode.

$\Delta V$ : the maximum voltage of the capacitor which can be reached during charging.

$V_{ref}$ : the reference voltage.

$C_{ext}$ : the added external capacitance.

Then the frequency of oscillation is denoted as

$$f_{osc} = \frac{I_{sense}}{2C_{ext}V_{ref}} \quad (4.15)$$

Thus, the oscillating frequency cannot be determined by the external capacitance but also the reference voltage. For example, by setting reference voltage at 1.3V, the output frequency is nearly halved compared with the original current-controlled oscillator.

To achieve outputting two unaliased signals with frequency up to 10 times above, the original current-controlled oscillator can only achieve 5 times large difference. However, the current controlled oscillator with modifiable reference voltage contains a comparator that encounters some problems when outputting high-frequency signals. If this oscillator work as amperometry, to linearly detect input current from 100pA to 10μA, the frequency range will be around 100dB, for instance ranging from 100Hz to 10MHz. The requirement for the comparator to handle MHz level signals is a large slew rate, hence a large bias current is needed contradicting the expected low power consumption. Therefore, this circuit can only be applied to low-speed potentiometric measurement.

### 4.3.3 simulation results

Potentiometric circuits combine the voltage to current converter and current controlled oscillator. As the simulation of voltage to current conversion is very linear as desired, the simulation of entire functional circuits needs to be done to prove the feasibility and performance of the potentiometric circuit. In comparator, M1, M2, and M3 work as a current source while M1 is connected with M6 which function as a linear resistor. To achieve low power consumption, the size of M6 is set to be 220nm/20um to have large resistance. M4 and M5 constitute a differential pair that is very sensitive to noise thus size are set to 60um/1um for better noise immunity, reduced mismatch influence as well as large amplification gain. M7 and M8 are an active load that also contribute to amplifying gain. M9 and M3 form a common source amplifier of which the gain is dependent on the biasing current and the aspect ratio of M9. Because this comparator is used in a very low-speed circuit indicating that power consumption is the priority which should be decreased as much as it can be even at the sacrifice of amplifying gain. As for the current-to-voltage converter, PM1-4 and NM1-4 are switches that are all set to be 2um/1um. The PM5-6 and NM5-6 are inverters which need to be tuned to have the switching point at half power supply voltage. The sizes of all transistors are listed in the table shown below.

Table 4.3: Sizes of transistors in the current to voltage converter

MOSFETs	W/L
M1	2um/1um
M2	4um/1um
M3	1um/4um
M4,M5	60um/1um
M6	220nm/20um
M7,M8	2um/10um
M9	2um/2um
PM1,PM2,PM3,PM4	2um/180nm
NM1,NM2,NM3,NM4	2um/180nm
PM5,PM6	6um/1um
NM5,NM6	1.65um/1um

The simulation are obtained and shown in Fig.4.14 when input voltage changes from 0.2V to 1.2V which has been confirmed with high linearity of voltage to current conversion.

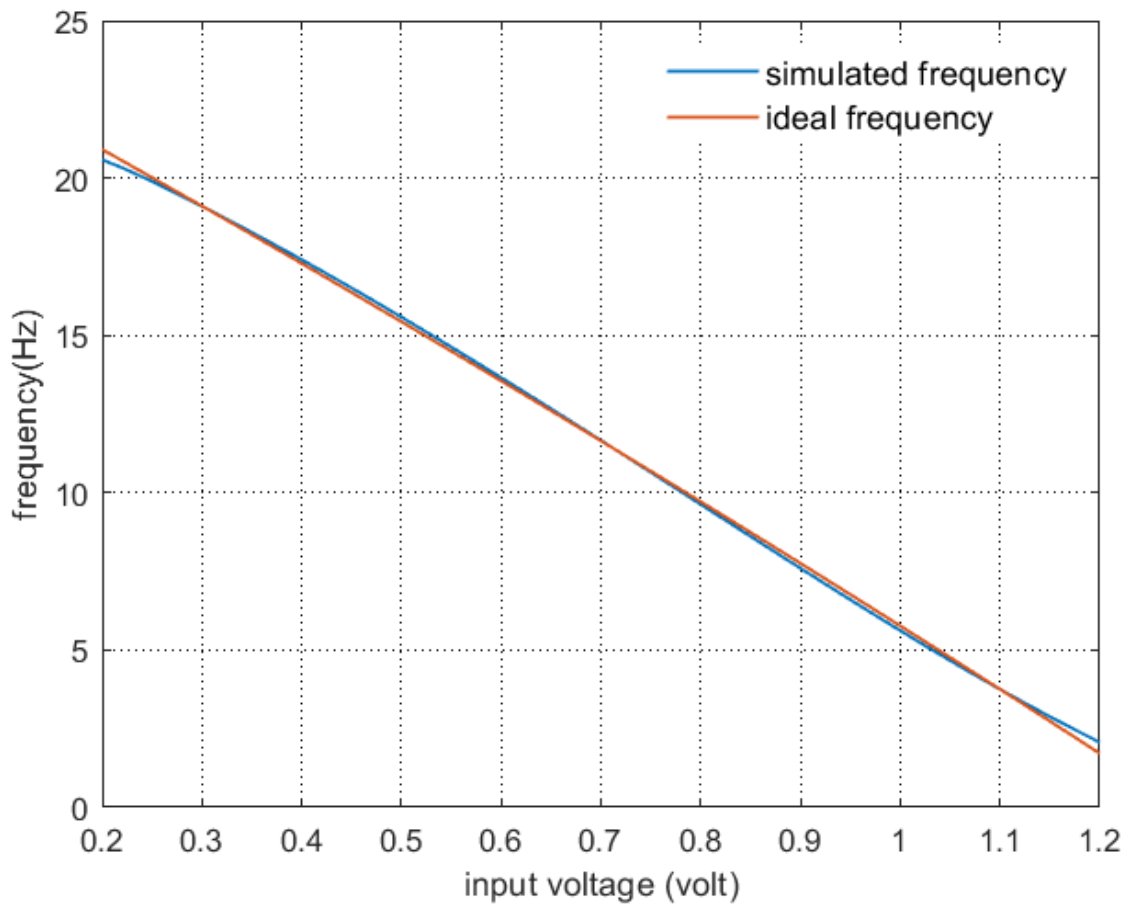


Figure 4.14: Systematic simulation on potentiometric circuit

The power consumption is shown below in Fig.4.15

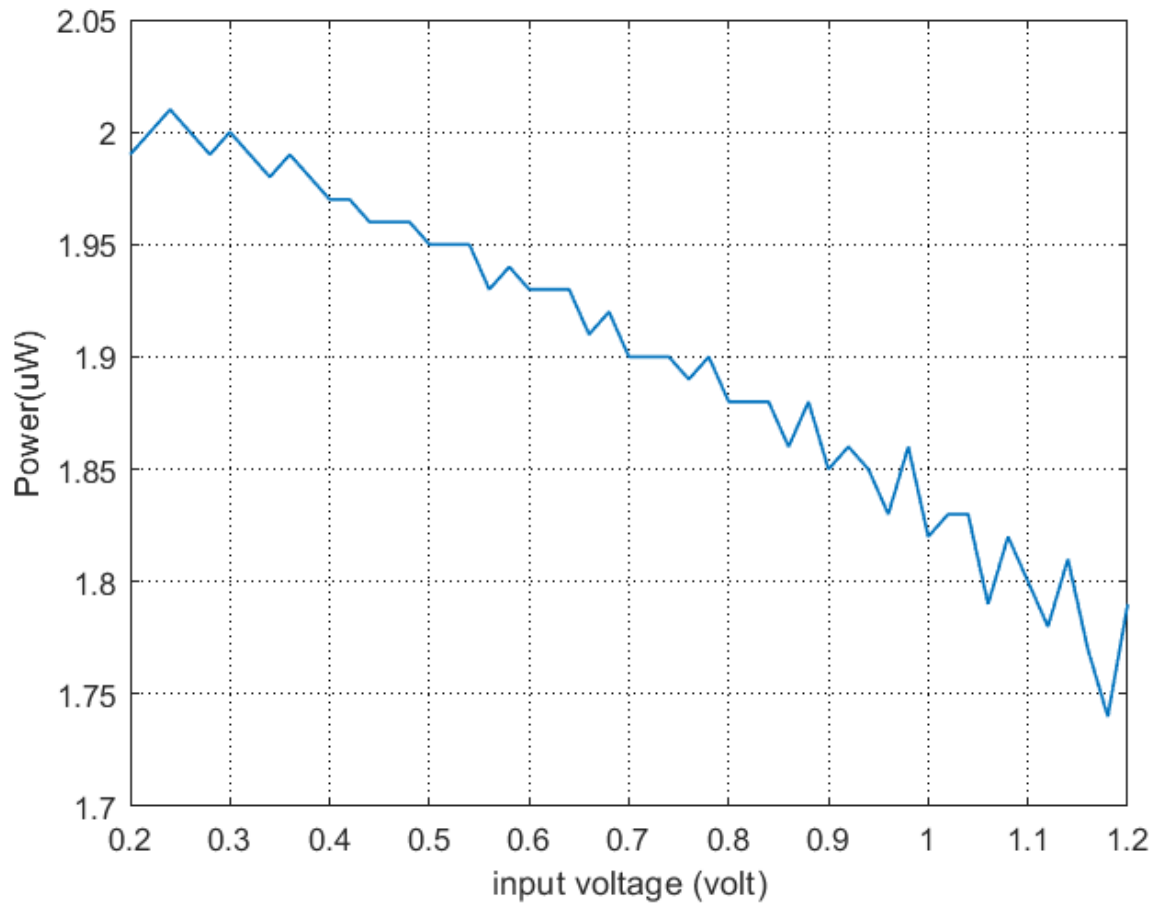


Figure 4.15: Power consumption of potentiometric circuit

The correlation between simulated curve and ideal curve is 0.9994. The output frequency ranges from 2.06Hz to 20.57HZ. The power consumption reaches the maximum  $2.01\mu W$  when input voltage is minimum.

#### 4.3.4 Overall simulation results

When combining the potentiometric and amperometric circuits in one system, the power consumption under different condition is shown in the table;

Table 4.4: Sizes of transistors in the current to voltage converter

input current	input voltage	power consumption
$6\mu A$	$0.2V$	$26.17\mu W$
$1\mu A$	$0.2V$	$12.24\mu W$
$0.5\mu A$	$1V$	$7.63\mu W$
$158pA$	$0.2V$	$3.76\mu W$
$0\mu A$	$0V$	$1.36\mu W$

The maximum frequency of potentiometry is  $20.57Hz@0.2V$  while the minimum frequency of amperometry is  $171Hz@100pA$  which does not conform to that the difference between frequency of two signals should be 10times larger. However, as the input current is  $158pA$  where frequency is  $277Hz$ , the frequency gap is larger than 10 times. Therefore the dynamic input range for input current is from  $158pA$  to  $6\mu A$  while potentiometric input ranges from  $0.2V$  to  $1.2V$

# Chapter 5

## Conclusion

### 5.1 Conclusion

**T**HIS thesis presents a novel concurrent amperometric and potentiometric measurement applied in portable biosensor. The biosensors consist of several components introduced in background while this work focuses on the readout circuit which processes the electrical signal in current and voltage domain input from electrodes by converting the signals into square-wave with different signals. By mixing up amperometric and potentiometric signals, the output of the system is transmitted through a single channel for easier processing and wireless data transmission.

The system's structure maintains the same as DAPPER sensing circuitry while proposing two different topologies of current-controlled oscillator, with one applied in amperometry, theoretically more area efficient due to small sizes of capacitors and small numbers of transistors, and another connected with an improved voltage-to-current converter to detect the sensing input voltage, outputting a low-frequency square-wave. The original DFF to mix up signals is replaced with a NAND gate, largely saving area and power.

The detailed simulation results of the innovative concurrent sensing circuits are presented in the thesis with improvement on expanding potentiometric input dynamic range from 0.4-1V

to 0.2-1.2V even with better linearity and amperometric input range dynamic range from 80p-1uA to 158p-6uA. The lower power consumption of system is realized by reducing maximum power consumption 16.71uW to 7.63uW under the same condition when input current is 0.5uA and input voltage is 1V. The circuit draws 26.7uW at maximum frequency which is slightly lower than initial design. The sensitivity of amperometry is very large that the gradient of the slope is 1644Hz/nA compared with 1260Hz/nA in initial design, with frequency ranging from 277Hz@158uA to 7.12MHz@5uA while frequency range in initial design is 214Hz@250pA to 551kHz@5.6uA.

## 5.2 Future Work

Because of time limitation of the project, There are some work listed below can be done in the future.

- The tape-out chips has been tested as malfunction due to minor design errors in PCB testing board, further tests are not carried out.
- The layout and post simulation of the proposed circuits needs to be done
- The voltage-to-current converter can be modified to provide positive linear response rather than negative linear response.
- Further investigation can be put on reduce the power consumption amperometric sensing as it increases exponentially when input sensing current reaches microampere level.
- More simulation on other characteristics of the sensor are required.
- Mixing signals techniques can be explored with possibility to mix up above two signals.

# Bibliography

- [1] V. Naresh and N. Lee, “A review on biosensors and recent development of nanostructured materials-enabled biosensors,” *Sensors (Switzerland)*, vol. 21, 2021.
- [2] Y. Xu, C. Li, W. Mei, M. Guo, and Y. Yang, “Equivalent circuit models for a biomembrane impedance sensor and analysis of electrochemical impedance spectra based on support vector regression,” *Medical and Biological Engineering and Computing*, 2019.
- [3] C. S. Lee, S. K. Kim, and M. Kim, “Ion-sensitive field-effect transistor for biological sensing,” 2009.
- [4] A. J. B. L. R. Faulkner, *ELECTROCHEMICAL METHODS Fundamentals and Applications Allen*, 2019, vol. 2.
- [5] C. Azcona, B. Calvo, S. Celma, and N. Medrano, “A novel rail-to-rail differential voltage-to-frequency converter for portable sensing systems,” 2012.
- [6] “Delta-sigma adc — digital-analog conversion — electronics textbook.” [Online]. Available: <https://www.allaboutcircuits.com/textbook/digital/chpt-13/delta-sigma-adc/>
- [7] R. J. Baker, *CMOS: Circuit Design, Layout, and Simulation: Third Edition*, 2011.
- [8] B. W. Ward, J. S. Schiller, and R. A. Goodman, “Multiple chronic conditions among us adults: A 2012 update,” *Preventing Chronic Disease*, vol. 11, 2014.
- [9] A. Sun, A. G. Venkatesh, and D. A. Hall, “A multi-technique reconfigurable electrochemical biosensor: Enabling personal health monitoring in mobile devices,” *IEEE Transactions on Biomedical Circuits and Systems*, vol. 10, 2016.

- [10] S. Kumar, S. Padmashree, and R. Jayalekshmi, "Correlation of salivary glucose, blood glucose and oral candidal carriage in the saliva of type 2 diabetics: A case-control study," *Contemporary Clinical Dentistry*, vol. 5, 2014.
- [11] S. Baliga, S. Muglikar, and R. Kale, "Salivary ph: A diagnostic biomarker," *Journal of Indian Society of Periodontology*, vol. 17, 2013.
- [12] D. A. Aikens, "Electrochemical methods, fundamentals and applications," *Journal of Chemical Education*, vol. 60, 1983.
- [13] M. J. Schöning, R. Krause, K. Block, M. Musahmeh, A. Mulchandani, and J. Wang, "A dual amperometric/potentiometric fia-based biosensor for the distinctive detection of organophosphorus pesticides," vol. 95, 2003.
- [14] J. E. Choi, J. N. Waddell, K. M. Lyons, and J. A. Kieser, "Intraoral ph and temperature during sleep with and without mouth breathing," *Journal of Oral Rehabilitation*, vol. 43, 2016.
- [15] K. Brunt, "Comparison between the performances of an electrochemical detector flow cell in a potentiometric and an amperometric measuring system using glucose as a test compound," *The Analyst*, vol. 107, 1982.
- [16] D. Ma, S. S. Ghoreishizadeh, and P. Georgiou, "Dapper: A low power, dual amperometric and potentiometric single-channel front end," vol. 2020-October, 2020.
- [17] A. Sadana, N. Sadana, and R. Sadana, "Economics of biosensors," 2018.
- [18] S. P. Mohanty and E. Kouciasanos, "Biosensors: A tutorial review," *IEEE Potentials*, vol. 25, 2006.
- [19] B. Jang and A. Hassibi, "Biosensor systems in standard cmos processes: Fact or fiction?" vol. 56, 2009.
- [20] C. N. Kotanen, F. G. Moussy, S. Carrara, and A. Guiseppi-Elie, "Implantable enzyme amperometric biosensors," *Biosensors and Bioelectronics*, vol. 35, 2012.

- [21] W. Cai, J. R. Peck, D. W. V. D. Weide, and R. J. Hamers, “Direct electrical detection of hybridization at dna-modified silicon surfaces,” *Biosensors and Bioelectronics*, vol. 19, 2004.
- [22] F. Ponzio and G. Jonsson, “A rapid and simple method for the determination of picogram levels of serotonin in brain tissue using liquid chromatography with electrochemical detection,” *Journal of Neurochemistry*, vol. 32, 1979.
- [23] E. B. Settingington and E. C. Alocilja, “Rapid electrochemical detection of polyaniline-labeled escherichia coli o157:h7,” *Biosensors and Bioelectronics*, vol. 26, 2011.
- [24] F. Usman, J. O. Dennis, A. Y. Ahmed, F. Meriaudeau, O. B. Ayodele, and A. A. Rabih, “A review of biosensors for non-invasive diabetes monitoring and screening in human exhaled breath,” *IEEE Access*, vol. 7, 2019.
- [25] C. Yang, S. R. Jadhav, R. M. Worden, and A. J. Mason, “Compact low-power impedance-to-digital converter for sensor array microsystems,” *IEEE Journal of Solid-State Circuits*, vol. 44, 2009.
- [26] L. Li, X. Liu, W. A. Qureshi, and A. J. Mason, “Cmos amperometric instrumentation and packaging for biosensor array applications,” vol. 5, 2011.
- [27] D. R. Thévenot, K. Toth, R. A. Durst, and G. S. Wilson, “Electrochemical biosensors: Recommended definitions and classification,” *Biosensors and Bioelectronics*, vol. 16, 2001.
- [28] L. R. F. A. J. Bard, *Electrochemical Methods: Fundamentals and Applications, 2nd Edition*, 2001.
- [29] G. W. Hunter, S. Akbar, S. Bhansali, M. Daniele, P. D. Erb, K. Johnson, C.-C. Liu, D. Miller, O. Oralkan, P. J. Hesketh, P. Manickam, and R. L. V. Wal, “Editors’ choice—critical review—a critical review of solid state gas sensors,” *Journal of The Electrochemical Society*, vol. 167, 2020.
- [30] R. I. Stefan, J. F. V. Staden, and H. Y. Aboul-Enein, “Immunosensors in clinical analysis,” vol. 366, 2000.

- [31] H. Komori, K. Niitsu, J. Tanaka, Y. Ishige, M. Kamahori, and K. Nakazato, "An extended-gate cmos sensor array with enzyme-immobilized microbeads for redox-potential glucose detection," 2014.
- [32] E. Barsoukov and J. R. Macdonald, *Impedance Spectroscopy: Theory, Experiment, and Applications*, 2005.
- [33] N. N. Mishra, S. Retterer, T. J. Zieziulewicz, M. Isaacson, D. Szarowski, D. E. Mousseau, D. A. Lawrence, and J. N. Turner, "On-chip micro-biosensor for the detection of human cd4+ cells based on ac impedance and optical analysis," *Biosensors and Bioelectronics*, vol. 21, 2005.
- [34] F. Yin, "A novel capacitive sensor based on human serum albumin-chelant complex as heavy metal ions chelating proteins," *Analytical Letters*, vol. 37, 2004.
- [35] M. Stelzle, G. Weissmüller, and E. Sackmann, "On the application of supported bilayers as receptive layers for biosensors with electrical detection," *Journal of Physical Chemistry*, vol. 97, 1993.
- [36] S. R. Lee, K. Sawada, H. Takao, and M. Ishida, "An enhanced glucose biosensor using charge transfer techniques," *Biosensors and Bioelectronics*, vol. 24, 2008.
- [37] S. Purushothaman, C. Toumazou, and C. P. Ou, "Protons and single nucleotide polymorphism detection: A simple use for the ion sensitive field effect transistor," *Sensors and Actuators, B: Chemical*, vol. 114, 2006.
- [38] E. P. Achterberg, "Laboratory techniques in electroanalytical chemistry," *TrAC Trends in Analytical Chemistry*, vol. 15, 1996.
- [39] A. Das, P. Bhadri, F. R. Beyette, A. Jang, P. Bishop, and W. Timmons, "A potentiometric sensor system with integrated circuitry for in situ environmental monitoring," vol. 2, 2006.
- [40] M. M. Ahmadi and G. A. Jullien, "Current-mirror-based potentiostats for three-electrode amperometric electrochemical sensors," *IEEE Transactions on Circuits and Systems I: Regular Papers*, vol. 56, 2009.

- [41] P. M. Levine, P. Gong, R. Levicky, and K. L. Shepard, "Active cmos sensor array for electrochemical biomolecular detection," vol. 43, 2008.
- [42] S. M. Martin, F. H. Gebara, T. D. Strong, and R. B. Brown, "A low-voltage, chemical sensor interface for systems-on-chip: The fully-differential potentiostat," vol. 4, 2004.
- [43] M. Crescentini, M. Bennati, M. Carminati, and M. Tartagni, "Noise limits of cmos current interfaces for biosensors: A review," *IEEE Transactions on Biomedical Circuits and Systems*, vol. 8, 2014.
- [44] D. Kim, B. Goldstein, W. Tang, F. J. Sigworth, and E. Culurciello, "Noise analysis and performance comparison of low current measurement systems for biomedical applications," *IEEE Transactions on Biomedical Circuits and Systems*, vol. 7, 2013.
- [45] H. M. Jafari and R. Genov, "Chopper-stabilized bidirectional current acquisition circuits for electrochemical amperometric biosensors," *IEEE Transactions on Circuits and Systems I: Regular Papers*, vol. 60, 2013.
- [46] H. Li, S. Parsnejad, and A. J. Mason, "Single ion channel cmos electrochemical instrument for high throughput recording arrays," vol. 2015-September, 2015.
- [47] H. Li, C. S. Boling, and A. J. Mason, "Cmos amperometric adc with high sensitivity, dynamic range and power efficiency for air quality monitoring," *IEEE Transactions on Biomedical Circuits and Systems*, vol. 10, 2016.
- [48] J. Guo, W. Ng, J. Yuan, S. Li, and M. Chan, "A 200-channel area-power-efficient chemical and electrical dual-mode acquisition ic for the study of neurodegenerative diseases," *IEEE Transactions on Biomedical Circuits and Systems*, vol. 10, 2016.
- [49] C. Stagni, C. Guiducci, L. Benini, B. Riccò, S. Carrara, B. Samorí, C. Paulus, M. Schienle, M. Augustyniak, and R. Thewes, "Cmos dna sensor array with integrated a/d conversion based on label-free capacitance measurement," vol. 41, 2006.

- 
- [50] M. H. Nazari, H. Mazhab-Jafari, L. Leng, A. Guenther, and R. Genov, "Cmos neurotransmitter microarray: 96-channel integrated potentiostat with on-die microsensors," *IEEE Transactions on Biomedical Circuits and Systems*, vol. 7, 2013.
- [51] P. Steegstra and E. Ahlberg, "Influence of oxidation state on the ph dependence of hydrous iridium oxide films," *Electrochimica Acta*, vol. 76, 2012.
- [52] B. Sundén, "Electrochemistry and thermodynamics," 2019.
- [53] I. Helm, L. Jalukse, and I. Leito, "Measurement uncertainty estimation in amperometric sensors: A tutorial review," 2010.
- [54] D. Ma, S. S. Ghoreishizadeh, and P. Georgiou, "Concurrent potentiometric and amperometric sensing with shared reference electrodes," *IEEE Sensors Journal*, vol. 21, 2021.